

The ^{85}Kr *s*-process Branching and the Mass of Carbon Stars

C. Abia¹

Dept. Física Teórica y del Cosmos, Universidad de Granada, E-18071 Granada, Spain.

`cabia@ugr.es`

M. Busso²

Osservatorio Astronomico di Torino, 10025 Pino Torinese, Italy

`busso@to.astro.it`

R. Gallino³

Dipartimento di Fisica Generale, Università di Torino, Via P. Giuria 1, 10125 Torino, Italy

`gallino@ph.unito.it`

I. Domínguez⁴

Dept. Física Teórica y del Cosmos, Universidad de Granada, E-18071 Granada, Spain

`inma@ugr.es`

O. Straniero⁵

Osservatorio Astronomico di Collurania, I-64100 Teramo, Italy

`straniero@astrte.te.astro.it`

and

J. Isern⁶

Institut d'Estudis Espacials de Catalunya - CSIC, Barcelona, Spain

`isern@ieec.fcr.es`

Received _____; accepted _____

ABSTRACT

We present new spectroscopic observations for a sample of C(N)-type red giants. These objects belong to the class of Asymptotic Giant Branch stars, experiencing thermal instabilities in the He-burning shell (thermal pulses). Mixing episodes called *third dredge-up* enrich the photosphere with newly synthesized ^{12}C in the He-rich zone, and this is the source of the high observed ratio between carbon and oxygen ($\text{C/O} \geq 1$ by number). Our spectroscopic abundance estimates confirm that, in agreement with the general understanding of the late evolutionary stages of low and intermediate mass stars, carbon enrichment is accompanied by the appearance of *s*-process elements in the photosphere. We discuss the details of the observations and of the derived abundances, focusing in particular on rubidium, a neutron-density sensitive element, and on the *s*-elements Sr, Y and Zr belonging to the first *s*-peak. The critical reaction branching at ^{85}Kr , which determines the relative enrichment of the studied species, is discussed. Subsequently, we compare our data with recent models for *s*-processing in Thermally Pulsing Asymptotic Giant Branch stars, at metallicities relevant for our sample. A remarkable agreement between model predictions and observations is found. Thanks to the different neutron density prevailing in low and intermediate mass stars, comparison with the models allows us to conclude that most C(N) stars are of low mass ($M \lesssim 3 M_{\odot}$). We also analyze the $^{12}\text{C}/^{13}\text{C}$ ratios measured, showing that most of them cannot be explained by canonical stellar models. We discuss how this fact would require the operation of an *ad hoc* additional mixing, currently called Cool Bottom Process, operating only in low mass stars during the first ascent of the red giant branch and, perhaps, also during the asymptotic giant branch.

Subject headings: nucleosynthesis — stars: abundances — stars: AGB — stars: carbon

1. Introduction

The production of elements heavier than iron is normally ascribed to neutron captures. At the low neutron density prevailing in Asymptotic Giant Branch (AGB) stars, this nucleosynthesis process is referred to as the *s-process*, where the neutron-capture path proceeds along the valley of β stability and most unstable isotopes encountered along the *s*-path preferentially β -decay instead of capturing a further neutron. However, in a number of cases, competition between neutron capture and beta decay leads to a *branching* in the synthesis path, which is determined by the neutron density and the neutron capture cross section of the unstable nucleus and its β -decay half-life (see e.g. Käppeler, Beer, & Wisshak 1989).

The discovery of the unstable element technetium in the spectra of AGB stars by Merrill (1952) clearly showed that the *s*-process actually occurs in these red giants of low to intermediate mass, $1.5 \lesssim M/M_{\odot} \lesssim 8$. The particular structure of AGB stars (two alternate burning shells, one of H and an inner one of He, surrounding an inert degenerate CO core) fulfills the necessary physical conditions for the *s*-process nucleosynthesis to occur. It is in the He-rich zone between the two burning shells (hereafter He intershell) that *s*-elements are produced by slow neutron captures on seed nuclei. Periodically the He intershell is swept by a convective instability induced by a He-burning runaway (thermal pulse, TP) where ^{12}C is synthesized. After each thermal instability, newly synthesized ^{12}C and *s*-elements are mixed with the envelope by a mixing episode called *third dredge-up*

(TDU) (Iben & Renzini 1983). The repeated action of TPs and TDU episodes during the AGB phase makes the star to eventually become carbon-rich, i.e. showing a ratio $C/O > 1$ in the envelope. Abundance studies of C-stars (N and SC types) in the Galaxy have indeed confirmed this figure (Utsumi 1985; Abia & Wallerstein 1998).

One debated subject concerning the *s*-process nucleosynthesis in AGB stars is the knowledge of the neutron source. Two competing sources have been envisaged: the $^{13}\text{C}(\alpha, n)^{16}\text{O}$ and the $^{22}\text{Ne}(\alpha, n)^{25}\text{Mg}$ reactions. During the last decade a number of studies in AGB stars of different spectral types have shown that the *s*-element abundance pattern can only be understood if the $^{13}\text{C}(\alpha, n)^{16}\text{O}$ reaction provides the bulk of the neutron flux at low neutron densities ($N_n \lesssim 10^7 \text{ cm}^{-3}$) and relatively low temperatures ($T \sim 1 \times 10^8 \text{ K}$) (cf. Wallerstein et al. 1997; Busso, Gallino, & Wasserburg 1999, and references therein). In AGB stars, this reaction occurs in radiative conditions during the interpulse phase, in the top layers of the He intershell (Straniero et al. 1995, 1997; Herwig et al. 1997; Gallino et al. 1998; Herwig 2000). In fact, the convective instability powered by a TP spreads over the whole He intershell the ^{12}C produced by the 3α reactions. When TDU takes place, a few amount of protons may diffuse from the H-rich envelope down to the He intershell. Then, during the interpulse, the region where these protons are stored heat up so that ^{13}C is rapidly formed, via proton captures on ^{12}C , and later on, when the temperature approaches 10^8 K , the $^{13}\text{C}(\alpha, n)^{16}\text{O}$ neutron source is activated (Busso, Gallino, & Wasserburg 1999).

On the other hand, the $^{22}\text{Ne}(\alpha, n)^{25}\text{Mg}$ neutron source requires higher temperatures ($T \gtrsim 3.5 \times 10^8 \text{ K}$), as those currently found in the TP of intermediate mass models (i.e. $M > 4 M_{\odot}$) (see e.g. Straniero et al. 2001). The maximum temperature achieved in low mass AGB stars (LMS) ($M \lesssim 3 M_{\odot}$) instead does not exceed $T \sim 3 \times 10^8 \text{ K}$ (Iben & Truran 1978; Straniero et al. 1997). Therefore, in LMS the ^{22}Ne neutron source is only marginally activated, and the ^{13}C source is the main supplier of neutrons. Conversely, in AGB stars of

$M \gtrsim 4 M_{\odot}$, both the ^{22}Ne and the ^{13}C neutron sources are efficiently activated, during the thermal pulse and during the interpulse, respectively.

The neutron burst by the ^{22}Ne neutron source occurs typically at high peak neutron densities, $N_n \gtrsim 10^{10} \text{ cm}^{-3}$ (see Vaglio et al. 1999; Busso, Gallino, & Wasserburg 1999). This strongly favors the production of the neutron-rich nuclides affected by the branching in the s -path, like ^{86}Kr , ^{87}Rb and ^{96}Zr . Therefore, a different s -element pattern is expected depending on whether one or the other neutron source is more active, thus allowing us to estimate the neutron density at the s -process site and consequently the initial AGB mass. The typical mass of the C-stars may be inferred by means of their luminosity distribution. In the LMC the C-stars luminosity function is peaked at $M_{\text{bol}} \sim -4.5$ (see e.g. Hughes & Wood 1990). A higher value ($M_{\text{bol}} \sim -5$) is found in the Milky Way. These luminosities are typical of low mass AGB stars. Very few C-stars have been found at $M_{\text{bol}} < -6$ (van Loon et al. 1998, 1999; Wallerstein & Knapp 1998; Trams et al. 1999), the mass of C-stars in the Magellanic Clouds being estimated to be lower than $2.7 M_{\odot}$ (Frogel, Mould, & Blanco 1990). Such an occurrence seems to exclude that stars with $M \gtrsim 4 M_{\odot}$ could become C-stars. However, it may be possible that the lack of bright C-stars is due to an observational selection effect: the brightest AGB stars could be obscured by an optically thick wind before they reach the $\text{C/O} > 1$ phase. On theoretical grounds, the question of the C-star mass has been a debated subject, because of the difficulty of finding TDU in LMS (Iben 1981). This problem has by now been overcome, since the TDU occurrence has been found in AGB stars with initial mass as low as $1.5 M_{\odot}$ (Lattanzio 1989; Straniero et al. 1997; Herwig 2000).

In addition, AGB stars of intermediate mass develop a large core mass ($M_{\text{H}} > 0.9 M_{\odot}$), and the temperature attained at the base of the convective envelope during the interpulse period becomes larger than $70 - 80 \times 10^6 \text{ K}$, so that ^{12}C is converted into ^{14}N . This is the

so-called Hot Bottom Burning (HBB, Sugimoto 1971; Iben 1975; cf. Iben & Renzini 1983) which is currently found in the most recent computations of intermediate mass AGB models (e.g. Blöcker & Schönberner 1991; Boothroyd, Sackmann, & Ahern 1993; Lattanzio et al. 1996; Forestini & Charbonnel 1997; Straniero et al. 2001). Such an occurrence could explain the lack of bright C-stars. However, the HBB efficiency also depends on the envelope mass. When, as a consequence of the mass loss, the mass of the envelope is reduced to $\sim 1.5 M_{\odot}$, HBB eventually ceases, while TDU continues to mix carbon from the He intershell with the surface (Boothroyd & Sackmann 1992; Frost et al. 1998). This could lead to the formation of a bright, possibly obscured, C-star. Note that during the HBB phase the $^{12}\text{C}/^{13}\text{C}$ ratio would remain very low and close to its equilibrium value of 3.5, and eventually rise up to 5 – 10 when $\text{C}/\text{O} \sim 1$ is achieved in the envelope (Lattanzio & Forestini 1998).

In this study abundances of Rb, Sr, Y and Zr in a sample of Galactic C-stars are simultaneously derived for the first time. By comparing these findings with those predicted by *s*-process nucleosynthesis models at the ^{85}Kr -branching in AGBs of different masses, we infer about the stellar mass of C-stars and the neutron source playing the main role in the *s*-process. In § 2 we describe the properties of the ^{85}Kr -branching. § 3 presents the observations and analysis. In § 4 the abundances derived in our sample of C-stars are discussed and compared with the *s*-elements abundance pattern found in others AGB-stars. Finally, in § 5 and § 6 we discuss the observational results in the framework of the current *s*-process nucleosynthesis models in LMS and IMS. Our conclusions are summarized in § 7.

2. The reaction branching at ^{85}Kr and the neutron density

The peculiarities of the neutron flow near the *magic* neutron number $N = 50$, and through the unstable ^{85}Kr in particular, offer the possibility of making an observational estimate of the neutron density. Neutron capture on ^{84}Kr leads either to the 10.7 yr ground

state of ^{85}Kr or to the 4.5 h isomeric state at 350 keV, which β -decays roughly by 80% to ^{85}Rb and by 20% to the ^{85}Kr ground state through a γ -transition. The production rate of $^{85}\text{Kr}^{iso}$ is quite important, amounting to about 50% of the total neutron capture cross section on ^{84}Kr . The half-life of the ground state of ^{85}Kr is long enough for the s -process flow to proceed further to ^{86}Kr and then to ^{87}Rb , in competition with β -decay to ^{85}Rb , depending on the neutron density. When the neutron density is higher than a few 10^8 cm^{-3} , the neutron channel is open and the s -process path feeds the neutron magic nuclei ^{86}Kr and ^{87}Rb . Since ^{85}Rb has a neutron capture cross section larger by a factor ~ 10 than ^{87}Rb , the total abundance of Rb as well as its isotopic mix is very sensitive to the neutron density. Indeed, the total Rb abundance can differ by one order of magnitude depending on whether the low or the high neutron density routing is at work (see Beer & Macklin 1989 for a detailed description of this branching). Therefore, the relative abundance of Rb to other elements in this region of the s -process path, such as Sr, Y and Zr, can be used to estimate the average neutron density of the s -process and, as a consequence, to infer the mass of the star. In fact, in the last 15 years this kind of study for Rb has been successfully performed in field stars (Tomkin & Lambert 1999) and in AGB stars of different spectral types: Ba stars (Tomkin & Lambert 1983; Malaney & Lambert 1988), MS and S giants (Lambert et al. 1995), yellow symbiotics (Smith et al. 1997) and some s -process-rich stars in ω Cen (Vanture, Wallerstein, & Brown 1994; Smith et al. 2000). These abundance studies have added further evidence favoring the $^{13}\text{C}(\alpha, n)^{16}\text{O}$ reaction as the neutron source. The observed sources in the above studies often belong to binary systems in which the companion is now a white dwarf (Jorissen et al. 1993). Thus, they owe the s -element overabundances to mass transfer from an ancient AGB star (the progenitor of the white dwarf companion) and not to an ongoing s -process. As to C(N) stars, the only spectroscopic estimates of s -process elements available so far are those by Utsumi (1985), which are however based on low-dispersion photographic plates, nor Rb was measured at the

time. With the improved set of spectroscopic data presented here we are able to determine the Rb abundance and to provide a much better estimate of Sr, Y, Zr, thus allowing us to examine the general problem of the initial mass also for the class of the C(N) stars.

3. Observations and analysis

The spectra of the C-stars analyzed in this study were taken at the Calar Alto Observatory using the 2.2 m telescope, and at the La Palma Observatory with the 4.2 m William Herschel telescope (WHT). They form part of a more extended study concerning the chemical composition of Galactic C-stars: see Abia & Wallerstein (1998), hereafter Paper I, and Abia & Isern (2000), hereafter Paper II. The echelle spectra obtained have a continuous coverage from $\lambda \sim 4000$ to 9000 \AA and a resolution $\lambda/\Delta\lambda = 40000$ for the Calar Alto spectra, or 60000 for those taken at WHT. The spectra are of good quality with S/N ratios from ~ 50 in the blue part of the spectrum, up to more than 100 in the red part. The spectra were reduced following standard techniques using the IRAF software package. To remove telluric absorptions, the reduced and calibrated spectra of the target stars were obtained by subtracting the spectrum of a bright, hot and rapidly rotating star.

The stellar parameters of the stars studied were derived in a similar way as in Paper II. In short: effective temperatures were mainly deduced from the calibration of the observed bolometric flux to the infrared flux in the L' -band ($3.7\mu\text{m}$) versus T_{eff} (stars marked with an asterisk in Table 1), or from the $(J - L')_o$ vs. T_{eff} calibration by Ohnaka & Tsuji (1996). Infrared photometry was taken from Fouqué et al. (1992) and Noguchi et al. (1981). When photometry was not available we adopted the T_{eff} values derived from angular diameter measurements (Dyck, van Belle, & Benson 1996). Otherwise, we adopted the value given in Lambert et al. (1986) for some stars in common with this work. We have used the grid of model atmospheres for C-stars computed by the Uppsala group (see Eriksson et

al. 1984, for details). These models cover the $T_{\text{eff}} = 2500 - 3100$ K, $C/O = 1.0 - 1.35$ ranges and all have the same gravity, $\log g = 0.0$. Considering the T_{eff} of the program stars and a typical luminosity $10^4 L_{\odot}$, this is a common value for AGB stars. Nevertheless, our gravity might be in error by as much as ± 1 dex due mainly to the uncertain estimate of the luminosity (M_{bol}). The CNO abundances in the model atmosphere of a given star were taken from the literature when available (Lambert et al. 1986), or estimated from spectral synthesis in the wavelength ranges analyzed here. The absolute abundances of CNO that can be estimated in that way are rather uncertain; however, the C/O ratio that mainly determines the global shape of the spectrum, is derived with good accuracy ($\sim \pm 0.05$). Whenever possible, $^{12}\text{C}/^{13}\text{C}$ ratios were obtained from our echelle spectra by synthetic fits to ^{13}CN features in the $7990 - 8040$ Å range following the same procedure as in Abia & Isern (1996). Otherwise, they were taken from the literature (Lambert et al. 1986; Ohnaka & Tsuji 1996). Some of the $^{12}\text{C}/^{13}\text{C}$ ratios derived here differ from those in Abia & Isern (1997) because of the different T_{eff} values and an updated CN and C_2 line list in the $7990 - 8040$ Å range used here. Finally, a typical microturbulence parameter of $\xi \sim 2.2$ km s $^{-1}$ was adopted in the analysis of all sample stars (Lambert et al. 1986). Table 1 shows the atmosphere parameters for the program stars.

The metallicity $[M/H]^1$ of our sample sources was derived from selected metallic lines in the stellar spectra (see Table 3). Most of these lines are located in the wavelength ranges $4450 - 4650$ Å and $4700 - 4950$ Å. In these wavelength windows, molecular absorptions are weak in C-stars and metallic lines can be identified more easily. The metallic lines were selected according to the same careful criteria described in Paper I. Most of the gf -values were taken from the literature or from the VALD (Piskunov et al. 1995) and Kurucz’s

¹We adopt here the usual notation $[X] \equiv \log (X)_{\text{program-star}} - \log (X)_{\text{comparison-star}}$ for the abundance of any element X.

CD-ROM No. 23 data bases. In some cases, we derived solar gf -values using the Holweger & Müller (1974) atmosphere model for the Sun. The abundances of metals were derived by the usual method of equivalent width measurements and curves of growth calculated in LTE. Upper limits to the equivalent widths (see Table 3) were not considered in deriving abundances. The $[M/H]$ value for each star in Table 2 is the mean value obtained from the selected metallic lines.

The abundances of the low-mass s -elements around the ^{85}Kr -branching (Rb, Sr, Y and Zr) were derived from spectroscopic features selected following the same criteria as those for metallic lines. Despite the fact that our C-stars show many heavy-element absorption lines, only a few of them were considered useful for abundance analysis. The reason of this is the severe blending with CN and C₂ lines, which is evident even at the high spectral resolution used here. The lines selected are shown in Table 3. Spectroscopic parameters were taken from the literature (see Table 3) since due to their weakness in the solar spectrum, the derivation of solar gf -values is very uncertain. Nevertheless, our gf -values are in very good agreement with the solar gf -values list derived by Thévenin (1989, 1990). For a sample of 30 lines in common we found a mean difference of 0.12 ± 0.20 dex. In a few cases, however, there is a significant difference which, in our opinion, clearly shows that the derivation of solar gf -values from very weak lines is not always safe. For instance, our main Y abundance indicator is the Y I line at 4819 Å. This feature is quoted with a 3 mÅ absorption in the Solar Spectrum Atlas by Moore, Minnaert & Hootgast (1966). However, Hannaford et al. (1982) note that the uncertainty in the wavelength of this line could be as high as 25 mÅ and very probably, Y being not the main contributor to this absorption in the Sun². In fact, using a solar gf -value for this line (~ 1 dex higher than the value in

²Indeed, the identification of this line as Y in the Solar Spectrum Atlas of Moore, Minnaert & Hootgast (1966) is quoted with a question mark.

Table 3) in the analysis of WZ Cas (our reference star, see below), we obtain a very low Y abundance ($[Y/H] \sim -1$) which is unrealistic given the near solar metallicity of this star and its level of heavy element enhancement (see Paper II). The same figure is found with two additional discrepant Ti I lines with the Thévenin’s list (at 4812 and 4821 Å): unrealistic Ti abundances are obtained in WZ Cas if solar gf -values are used (the absorptions in the Sun are 8.5 and 3 mÅ, respectively). Finally, our gf -value of the Fe I line at 5848 Å also differ significantly with that by Thevenin. However, the iron abundance derived from this line in the only star where it is identified (Z Psc), is in agreement within ± 0.2 dex with that derived from other Fe lines in this star.

Abundances of s-elements were also derived from curves of growth in LTE except for those lines presenting clear blends, namely: the 7800 Å Rb I, 7070 Å Sr I and 4815.05, 4815.65 Å Zr I lines, for which we used spectral synthesis (see Table 3). CN and C₂ lines in these wavelength ranges were kindly provided by B. Plez and P. de Laverny according to the spectroscopic predictions by de Laverny & Gustafsson (1998). Final individual abundances were obtained as the mean of the abundances derived from each line. Unfortunately, given the important error in the measurement of the equivalent widths and the small number of lines used, it was impossible to check the atmospheric parameters (T_{eff} , $\log g$ and ξ) using the requirement that individual abundances derived from lines of different intensity, ionization state and excitation energy, have to be nearly equal.

In order to reduce systematic errors due to wrong gf -values and departures from LTE, certainly present in late-type giants (Tomkin & Lambert 1983), we performed a differential analysis line-by-line using WZ Cas (C9,2J; SC7/10) as the comparison star. This star has a similar T_{eff} and surface gravity as the stars studied here and its spectrum is also dominated by CN and C₂ absorptions. However, because the C/O ratio in its atmosphere is very close to unity (C/O ≈ 1.005) the spectrum is less crowded with molecular absorptions,

and thus the atomic line identification is easier. This permits a more accurate abundance analysis. Abundance studies of this star reveal that its metallicity is almost solar, $[\text{Fe}/\text{H}] \approx 0.0$ (Lambert et al. 1986; Paper II), with no or very small *s*-element overabundances: the mean heavy element enhancement is $[\text{h}/\text{Fe}] = 0.02 \pm 0.20$, where ‘h’ includes Sr, Y, Zr, Nb, Ba, La, Ce, and Pr (see Paper II). All the abundance ratios shown in Table 2 are relative to WZ Cas³.

The derivation of the Rb abundance requires special attention. In C-stars the line used here is strongly blended with CN, C₂ lines and some atomic absorptions. Therefore, the Rb abundance must be derived by spectral synthesis. We have used an updated version of the molecular and atomic line list used in Papers I and II. The new line list includes some additional ¹²C¹⁵N, ¹³C¹⁵N and ¹³C¹³C lines computed by B. Plez. We have also modified the *gf*-value of a weak Si I line to the blue of the Rb line according to Tomkin & Lambert (1999). The hyperfine structure of the Rb I line was considered adopting a Solar System isotopic ratio ⁸⁵Rb/⁸⁷Rb = 2.59 (Anders & Grevesse 1989). Note that the isotopic Rb mixture can certainly be altered as a function of the neutron density in the stars. Unfortunately, this isotopic ratio cannot be measured spectroscopically. Nevertheless, we checked that other isotopic mixtures will not change significantly our conclusions (see below). We have adopted the meteoritic Rb abundance, $\log (\text{Rb}/\text{H}) + 12 = 2.40 \pm 0.05$ (Anders & Grevesse 1989). We preferred to adopt the meteoritic abundance rather than

³The $[\text{h}/\text{Fe}]$ value in WZ Cas differs slightly from that derived in Paper II $[\text{h}/\text{Fe}] = +0.16$, because of the downward revised Sr, Ba and La abundances here. This new analysis was done with a very high resolution spectrum ($R \sim 180000$, $S/N > 70$) obtained, for another scientific purpose, with the 2.5 m NOT and the SOFIN echelle spectrograph at La Palma Observatory. In the re-analysis of WZ Cas we have used Sr, Ba and La lines mainly placed in the 4800 – 4950 Å spectral range.

the photospheric one (2.60 ± 0.15) as the reference value because of the weakness of the 7800 Å Rb I line in the Sun ($< 1 \text{ m}\text{\AA}$) from which the photospheric abundance is derived. Instrumental and macroturbulence broadening were included in the Rb synthesis. The macroturbulence broadening was set by matching the profile of an almost clean nearby Ni I line at 7788.9 Å.

A striking result immediately appears in the analysis of the 7800 Å Rb I line: the Rb abundances derived are unrealistically low considering the near-solar metallicity of most C-stars analyzed here. In fact, the derived abundances of Rb are lower than solar by a factor ranging typically between four and ten. This figure has also been found in similar studies on AGB stars (Plez, Smith, & Lambert 1993; Lambert et al. 1995; Abia & Isern 2000). The reason for this is not well understood, although N-LTE effects due to overionization might partially explain this finding. In fact, due to its low ionization energy (4.16 eV), rubidium is mostly ionized at the depth of the 7800 Å line formation. Abia, Pavlenko, & de Laverny (1999) showed that N-LTE effects in C stars due to overionization in the formation of the resonance Li I at 6708 Å (another alkali element with an ionization energy similar to Rb, 5.39 eV) might extend up to +0.6 dex (in the sense of N-LTE minus LTE abundances). Surprisingly, the same effect is found when deriving K abundances (ionization energy 4.34 eV) from a nearby resonance K I line at 7698.70 Å; the K abundances derived are also unrealistically low: typically $[\text{K}/\text{H}] \sim -1^4$. No nuclear process able to deplete K in stars is known. Although both the Li and K lines are usually stronger than the Rb I line in C-stars and, in consequence, they should form higher in the atmosphere where larger departures from LTE are expected, upward corrections of the Rb abundance are not excluded until

⁴Certainly N-LTE effects are important in the formation of the resonance 7698 Å K I line in the Sun (Takeda et al. 1996). However, as far as we know, there is no a similar study in C-rich giants.

a quantitative analysis of N-LTE effects in the resonance Rb line is made. However, we believe that N-LTE effects are not probably the full story. In our opinion there also seems to be a problem related to the continuum opacity in the 7800 Å region. Indeed, the metallicity derived from (almost unblended) Ni I and Fe I lines near the Rb I line is significantly lower (by a few tenths of dex) than the one derived from the metallic lines in the blue part of the spectrum. This suggests that the continuum absorption coefficient of the real atmosphere in the Rb spectral region is not well reproduced by our model atmospheres. Tests made by modifying the model atmosphere parameters in a quantity similar to the expected errors (see Table 4) do not solve the problem. However, when trying to artificially simulate this missing opacity by increasing the H^- opacity (namely, increasing the electronic pressure in the model atmosphere), the derived metallic and Rb abundances increase by tenths of dex. Again, we have to wait for improved model atmospheres of C-stars (Plez 1999) to study this problem better. Therefore, because of the uncertain Rb abundances, we computed the [Rb/M] ratio using the metallicity ([M/H]) derived from the metallic lines close to the Rb line. The [Rb/M] ratios in Table 2 were computed in that way, also using WZ Cas as the comparison star.

Unlike Rb, strontium has many spectroscopically accessible lines. However, in C-stars most of them are very strong and/or located in crowded regions of atomic and molecular absorptions. As the main indicator of the Sr abundance we have used the Sr I line at 7070.1 Å. In some of the stars observed at a very high resolution ($R \sim 60000$), it was possible to derive Sr abundances from two additional Sr I lines at 4811 and 4872 Å. In the neighbourhood of these lines, however, the continuum position is uncertain. The Sr I line at 7070 Å is blended with some ^{13}CN lines of moderate intensity, so that spectral synthesis is required. We obtain a solar gf -value for this line from the solar spectrum using the photospheric Sr abundance 2.90 ± 0.06 (Anders & Grevesse 1989). No hyperfine structure was considered for the 7070 Å Sr I line, since this absorption is rather weak

($\log W_\lambda/\lambda \lesssim -4.5$) even in C-stars with large Sr enhancements. Due to the blend with ^{13}CN lines, the abundance of Sr derived from this feature is sensitive to the $^{12}\text{C}/^{13}\text{C}$ ratio adopted. Unfortunately, given the current uncertainties in the derivation of CNO abundances and the atmospheric parameters of C-stars, the typical error in the derivation of the $^{12}\text{C}/^{13}\text{C}$ ratio is still high, $\pm(6 - 13)$: the higher the $^{12}\text{C}/^{13}\text{C}$ ratio, the higher the error (see Abia & Isern 1996). This introduces an extra uncertainty into the derivation of the Sr abundance from this line, mainly in stars with $^{12}\text{C}/^{13}\text{C} \lesssim 30$. Therefore, the $[\text{Sr}/\text{M}]$ ratios derived here have to be considered with some caution⁵. On the other hand, synthetic fits in the Sr spectral range include a clean Ti I line at 7065.50 Å that was used as an additional check to the $[\text{M}/\text{H}]$ ratio derived from metallic lines in the blue part of the spectrum and to set the macroturbulence broadening.

3.1. Errors

Errors involved in the derivation of abundances in C-stars are large. The sensitivity of the derived abundance ratios to the model atmospheres was assessed by changing the atmospheric parameters over a plausible range of T_{eff} , ξ , CNO abundances, C/O and $^{12}\text{C}/^{13}\text{C}$ ratios. Obviously, for a given element the change in the abundance created by varying each atmospheric quantity depends on the excitation energy and on the intensity of the specific line (we have used only neutral lines). In Table 4 we show the sensitivity of the $[\text{X}/\text{H}]$ ratios to the above sources of error. We have also included the error introduced by an uncertainty of 5% in the location of the continuum in the spectrum (if spectral synthesis

⁵Nevertheless, in the stars where it was possible to derive Sr abundances from the lines in the blue, the dispersion never exceeded ± 0.3 dex, which is consistent with the expected total error.

is used) or due to errors in the equivalent width measurements (when curves of growth are used). We do not include the effect of uncertainties in the gravity since we have only atmosphere models computed with $\log g = 0.0$. However, since we have used only neutral lines in the analysis, our abundances would not be very sensitive to changes in gravity within a variation of ± 0.5 dex in $\log g$. The values reported in Table 4 were computed using equivalent widths and model atmosphere parameters that are representative in the program stars, namely: $-\log W_\lambda/\lambda = 4.3$ to 5.0 , $T_{\text{eff}} = 2850$ K, $\log g = 0.0$, $\xi = 2.2$ km s $^{-1}$, C/O = 1.05 and $^{12}\text{C}/^{13}\text{C} = 40$. From this table it is apparent that the mean sources of error come from uncertainties in T_{eff} , microturbulence and errors in the equivalent width measurement or the spectral synthesis fit (by eye). Indeed, the microturbulence in variable stars might differ with wavelength in the spectrum (due to differences in depth of line formation), and might change with the pulsation phase of the star. We believe, however, that an uncertainty in the microturbulence as large as ± 1 kms $^{-1}$ can be discarded because this can be checked from synthetic fits to CN lines in the spectral regions studied. For instance, synthetic fits to the strong and crowded CN lines in the 7070 Å region show that such a variation respect to our adopted value (2.2 kms $^{-1}$) would either result in CN lines that are too narrow and free of significant blending with adjacent lines, or produce extreme saturation effects. In the former case, the convolution parameters required to fit the spectrum would be very large. In the later, the resulting spectrum would be very smooth with an unrealistic continuum position. Furthermore, the effect of variations in the microturbulence may also be distinguished from that of variations in the C/O ratio since the former deepen and become broader and more blended with the neighboring features. We note that Lambert et al. (1986), analyzing weak CO and CN lines ($\log (W_\lambda/\lambda) \lesssim -4.5$) in a sample of 30 C-stars (many of them studied here), obtain a mean value $\xi = 2.16 \pm 0.20$ kms $^{-1}$. On the other hand, note from Table 4 the small sensitivity of the Y and Zr abundances and metallicity to uncertainties in the C/O, $^{12}\text{C}/^{13}\text{C}$ and CNO/H ratios. This is because these abundances

are derived using curves of growth from unblended (with CN or C₂ features, as far as our molecular line lists indicate) lines.

The quoted accuracy of our *gf*-values range between 5% – 25%, which is translated to an error in the derived abundances between 0.05-0.25 dex depending on the intensity of the line. However, as all the abundances derived here are set in ratio to WZ Cas, errors in the *gf*-values are not the relevant ingredient. More important is the random error in the abundance of elements represented by a few number of lines or just one. In this case, the quality of the lines in question is the critical point. For instance, we consider the 7800 Å Rb I line as a good indicator since our synthetic spectra reproduce quite well this spectral region. The same applies for the Zr I blend at 4815 Å and for the Y I line at 4819 Å, which appears safely clean of blends in the majority of the spectra. In any case, an estimate of this random error can be evaluated from the resulting dispersion around the mean abundance value in the cases where more than three lines are used. This can be done for a few stars (see Table 3) and only for Ti and Fe abundances. We found a dispersion in the range 0.1-0.25 dex. On the other hand, systematic errors, not included in Table 4, may be present affecting the [X/M] ratios. The leading contributor to a systematic error is probably our assumption that N-LTE effects are reduced when the program stars are analyzed with respect to WZ Cas. Note also that our stars are variable, therefore, the effective temperature might change with the pulsational phase. The quoted ΔT_{eff} in Table 4, thus, refers to the typical expected uncertainty in the derivation of this parameter according to the different methods used: photometry, infrared flux or angular diameter measurements (see above). Focusing on Rb for instance, a Rb isotopic mix different than solar would modify the derived Rb abundance. Nevertheless, variations of the ⁸⁵Rb/⁸⁷Rb by a factor of five implies a maximum variation of only ± 0.1 dex in the Rb abundance. On the other hand, if the solar photospheric Rb abundance is preferred as a reference, the [Rb/M] ratios in Table 2 have to be reduced by 0.2 dex. Other sources of error such as the

uncertainty in the model atmospheres (hydrostatic plano-parallel approximation, velocity stratifications, poly-atomic opacities), dust or chromospheres are at present impossible to quantify. We estimate a total typical error (non systematic) of ± 0.30 dex for $[M/H]$, ± 0.30 dex for $[Rb/H]$, ± 0.35 dex for $[Sr/H]$, ± 0.30 dex for $[Y/H]$, and ± 0.40 dex for $[Zr/H]$.

Adding-up quadratically to these figures the random error due to the use of a few number of lines, the total error in the $[X/H]$ ratios would range between ± 0.3 - 0.45 dex. Errors in the $[X/M]$ and $[X/Y]$ ratios are, in general, lower since these ratios are less sensitive than the $[X/H]$ ratios to the atmosphere parameters: sources of error affecting in the $[X/H]$ ratios to the same sense cancel out when computing these element abundance ratios.

Below, we compare our results with previous abundance analyses and with theoretical predictions of *s*-process nucleosynthesis in C-stars of different masses.

4. The abundance ratios and their characteristics

A detailed chemical analysis of heavy element abundances from Rb to Ce in a larger sample of Galactic C(N)-stars will be presented in a forthcoming paper (Abia et al. 2001, in preparation). Here we restrict the discussion to the low-mass *s*-elements (Rb, Sr, Y and Zr). Table 2 shows the abundance ratios with respect to the metallicity derived in our stars referred to WZ Cas. Most stars are of near-solar metallicity, except V CrB and IY Hya, which can be considered as metal-poor C-stars (see below). The stars present moderate light *s*-element (Zr, Y, Sr) enhancements, namely: $\langle [Rb/M] \rangle = 0.27 \pm 0.24$, $\langle [Sr/M] \rangle = 0.41 \pm 0.19$, $\langle [Y/M] \rangle = 0.59 \pm 0.17$ and $\langle [Zr/M] \rangle = 0.54 \pm 0.22$. These overabundances are significantly lower than those reported by Utsumi (1985) in a similar analysis. Excluding Rb (not studied by Utsumi), our $[ls/M]$ ratios, with ‘ls’ = (Sr, Y, Zr), are 0.4 – 0.6 dex smaller. However, as discussed in Paper II, the abundances derived by Utsumi (1985) were based on atomic line identifications made in a previous work (Utsumi

1970), and indeed most of the heavy-element lines identified in this work appear as clear blends at the spectral resolution used here (a factor three higher than Utsumi’s one). This necessarily leads to abundance overestimations. Additionally, Utsumi used in his analysis the Allen’s (1976) Solar System abundances as reference values, which are lower by 0.05 (Sr), 0.44 (Y) and 0.1 (Zr) dex than the reference values used here (Anders & Grevesse 1989). This explains part of the differences found with respect to Utsumi’s analysis.

In any case, the light *s*-element abundance ratios derived here are lower than previously thought and contrast with the higher overabundances found in other C-rich *s*-enhanced stars or their descendants (Ba , CH and SC-stars: see for instance Vanture 1992a,b; Smith & Lambert 1988), and in fact are more similar to the findings of O-rich S stars (Smith & Lambert 1990). We remind that during the AGB phase it is commonly assumed that the abundance of ^{12}C and *s*-elements increases in the envelope of the star along the spectral sequence $\text{M} \rightarrow \text{MS} \rightarrow \text{S} \rightarrow \text{SC} \rightarrow \text{C}$. As the TP and TDU episodes occur repeatedly, and since most of our stars have C/O ratios near unity, they should show abundances similar to those found in SC-stars⁶. However, comparison with the average low-mass *s*-element enhancements found in SC-stars (see Paper I) shows a difference of about +0.5 dex, in the sense of SC-stars minus C(N)-stars. We believe that this difference is due to several reasons. First, the abundances in Paper I were derived from lower resolution spectra (a factor ~ 2). Second, despite the fact that SC stars show less intense molecular absorptions (CN & C₂), due to their C/O ratio being very close to unity, the abundance analysis in Paper I was based on atomic lines identified in spectral ranges (5900 – 8000 Å) that were much more crowded with molecular absorptions than those mainly used here (4750 – 4950 Å). These two

⁶SC-stars are AGB stars with a C/O ratio very close to unity within 1% or less. Furthermore, they show spectroscopic characteristics which are used to distinguish them from the C(N)-stars (see Keenan & Boeshaar 1980, for a complete definition).

facts might have produced systematic abundance overestimates due to undetected blends. However, the main reason is probably due to differences in the model atmospheres used. In Paper I atmosphere models for SC-stars from D. Alexander (private communication) were used. We checked that for the same atmosphere parameters, the thermal structure in the higher layers differs significantly from that obtained in the Uppsala models used here. In fact, the abundances derived using Alexander’s models differ from those derived using the Uppsala models by 0.4 to 0.7 dex!, in the sense of Alexander minus Uppsala abundances: the lower the excitation energy of the line, the higher the abundance difference is. This affects the *s*-elements abundance estimates more than the metallic abundances, since the latter are derived from higher excitation energy lines. If this effect were considered, the $[X/M]$ ratios in our stars would have to be increased (or decreased in SC-stars) systematically by 0.3 to 0.5 dex depending on the individual element. In that case SC- and C(N)-stars *s*-element overabundances can be estimated at similar levels within the error bars. This fact is a clear example of the large uncertainties involved in the chemical analysis of AGB stars.

As to the class of MS/S stars, which are almost as close to solar metallicity as the present sample of C-stars, the average $\langle [ls/Fe] \rangle$ is +0.7, with a typical uncertainty of 0.25 dex (Busso et al. 2001). Within the respective uncertainties they have therefore enhancements very similar to those of C(N) stars in the present paper. With respect to the warmer BaII giants in the disk, which show $\langle [Fe/H] \rangle = -0.3$, the subsample with $[Fe/H] > -0.3$, amounting to 8 stars in the selection made by Busso et al. (2001), gives $\langle [ls/Fe] \rangle = +0.85$. Actually, the Ba stars are considered to be extrinsic AGBs, i.e. binary systems in which the present giant was enriched in *s*-elements by mass transfer from the primary AGB star. This means that the original AGB envelope must have been even more enriched in low-mass *s*-elements, by a factor of at least 0.2 dex. The present sample of C-stars as well as that of similar *s*-enriched stars is not an ample one and the average values should be taken with some caution. Furthermore, both the MS/S and the C-stars show

more complex spectra crowded by molecular lines than the warmer Ba II giants, which are also less C-rich. Summing up, we shall have to wait for more ample statistics and refined model atmospheres of the C-rich stars to make further inferences in these comparisons.

Three stars in the sample, V CrB, VX Gem and IY Hya, deserve special attention. The first two stars are Mira variables with periods of 357 and 379 days, respectively. For the Mira variable V CrB, Kipper (1998) derived $[\text{Fe}/\text{H}] = -2.12$ and $[\text{ls}/\text{Fe}] \approx +1.5$ and concluded that the abundance pattern in this star is similar to that of other late-type CH-stars. The values we derived in this star for these figures are very different (see Table 2). We do not have an easy explanation for this discrepancy, as we used the same model atmosphere (kindly provided by T. Kipper). Because of T_{eff} variations in Mira variables, we have analyzed this star using other T_{eff} values as proposed in the literature (see discussion in Kipper’s paper). However, the best fit to the observed spectrum is obtained with the value adopted here, $T_{\text{eff}} = 2250$ K. Inspection of Figure 3 in Kipper (1998) makes clear that the heavy element abundances derived by spectral synthesis just fit the cores of the absorption lines without reproducing consistently the global behavior of the observed spectrum. We thus believe that the line list used in Kipper’s analysis of V CrB does not contain important CN and C₂ absorption, what unavoidably leads to the derivation of larger $[\text{X}/\text{Fe}]$ ratios. This could be the reason for the important differences between the two analyses.

Also for the Mira variable VX Gem the spectroscopic abundance analysis is rather complex. This star shows line-doubling in the stronger lines (Na I D doublet, 7698 Å K I, 6708 Å Li I). The hydrogen lines (α, β, γ) as well as the 5980 Å Mg I line are in emission. The Ca II infrared triplet shows P-Cygni profiles. All these features indicate the existence of a circumstellar envelope. On the other hand, T_{eff} for this star is rather uncertain. We have adopted 2500 K according to the analysis of Groenewegen et al. (1989), but Ohnaka & Tsuji (1996) derived 3050 K from infrared photometry and classified this star as a

SC-star. Indeed, effective temperatures in Mira variables change during the pulsational phase. However, we have found a better agreement between the theoretical and the observed spectrum in all the spectral ranges analyzed when adopting $T_{\text{eff}} = 2500$ K. The abundances derived in this star therefore have to be considered with caution. In fact, although the Rb I line is clearly visible in its spectrum we prefer not to estimate the [Rb/M] ratio because of the probable contamination with a circumstellar Rb line.

The situation concerning IY Hya is even more confusing. This star is a very red object with a high mass-loss rate, $4 \times 10^{-6} M_{\odot} \text{ yr}^{-1}$ (Jura & Kleinmann 1989). Furthermore, IY Hya is one of the few Galactic super Li-rich C(N)-stars, with $\log(\text{Li}/\text{H}) + 12 \sim 4.0$ (Abia, Pavlenko, & de Laverny 1999). The atmosphere parameters for this star are quite uncertain since no direct determination exists in the literature. Evidence of this is the fact that we do not find a unique CNO abundance choice (within error bars) that would give a good fit for all the spectral ranges analyzed here. Thus, because of the very uncertain abundance ratios derived in V CrB, VX Gem and IY Hya, we have plotted their abundance ratios with smaller symbols in the figures below, to indicate that they have a lower weight in our analysis.

4.1. Technetium

As an additional hint to the abundance pattern found in our stars we searched for the presence of technetium. The search was based mainly on the analysis of the intercombination Tc I line at 5924.47 \AA (see Paper I for a detailed explanation of the procedure followed in the analysis of this Tc blend). Unfortunately, the stronger resonance Tc lines around 4260 \AA are inaccessible in most C-stars because of the strong flux depression in these stars below $\sim 4400 \text{ \AA}$. In the last column of Table 2 we have indicated whether or not Tc is identified for each star. A “yes” entry means that the best fit to the 5924 \AA blend

is obtained when a Tc abundance different from zero is used in the spectral synthesis⁷. With a “no” entry we mean that a synthetic spectrum with no-Tc does not significantly differ from another one computed with a very small Tc abundance. In some stars the best fit to the Tc blend is obtained using a small Tc abundance but not strictly zero. These stars have been quoted with a “doubtful” (dbfl) entry since in our judgment the evidence favours the absence of Tc. We have to note however, that a “no” in Table 2 does not necessarily mean that Tc is absent since, as the 5924 Å Tc I line is much weaker and in a more crowded zone than the resonance lines near 4260 Å, a detailed study of the latter might eventually reveal the presence of Tc. Nevertheless, in two stars for which it was possible to analyze both the 5924 Å and 4260 Å spectral ranges (VX Gem and W Ori), we reached the same conclusion for both lines (see Table 2). If we exclude the stars quoted as doubtful, 50% of the stars in Table 2 show Tc, the others are compatible with a non-detection. Interestingly enough, the same figure is found in MS/S stars with/without Tc (Smith & Lambert 1985, 1986, 1990). If one applies the same rules currently accepted for the MS/S giants to our C-rich objects, then Tc-no C(N)-stars would be extrinsic AGBs (candidates to have a WD companion), with extra dilution of *s*-element abundances related to mass transfer from a companion. However, we do not find any correlation between the level of heavy-element enhancements and the presence of Tc. In fact, for the Tc-yes and Tc-no stars we found $\langle [ls/Fe] \rangle = +0.53$ and $\langle [ls/M] \rangle = +0.48$, respectively.

As far as we know, there is no evidence of binarity for any of the stars studied here; despite this, we can take a further step in order to identify the extrinsic (binary) or intrinsic nature of our C-stars by studying their IR colours in the same way as Jorissen et al. (1993) did for S-stars. Infrared colours provide a measure of the optical properties

⁷Examples of the quality of the fits to the Rb and Tc blends can be appreciated in the corresponding figures shown in Papers I and II.

of circumstellar dust. Such dust is expected to be around intrinsic (non-binary) C-stars, and thus the presence or absence of dust emission might enable us to discriminate between intrinsic and extrinsic C-stars. Following the results of Jorissen et al. (1993) most Tc-rich S stars have IR excesses ($R \gtrsim 0.1$), which would indicate that they owe their chemical peculiarities to intrinsic nucleosynthesis processes. On the contrary, Tc-deficient (binary) S stars usually show $R < 0.1$. To estimate this IR excess due to dust, the flux ratios $R = F(12\mu\text{m})/F(2.2\mu\text{m})$ were computed. The 2.2 μm infrared flux was derived from the K magnitude taken from the Two Micron Sky Survey (Neugebauer & Leighton 1969; Claussen et al. 1987) and the 12 μm fluxes from the IRAS point source catalogue. The small sample of C-stars and the fact that our Tc analysis is based on a weak line in a crowded zone prevents us from reaching any firm conclusion. However, we find that 72% of Tc-no stars in Table 2 have $R < 0.1$, while this figure decreases to 45% in the Tc-yes stars. This may be an indication of some correlation in the same direction as found in S stars. A similar study in a larger sample of C-stars is clearly necessary.

5. The stellar and nucleosynthesis reference models

In order to compare our observed abundances of C(N)-stars with predictions from current models of AGB evolution and nucleosynthesis, we use the *s*-process nucleosynthesis results from Gallino et al. (1998), Travaglio et al. (2001) and Busso et al. (2001), which are based on a large set of AGB stellar models, for stars of initial mass between 1.5 and 7 M_{\odot} , made with the FRANEC evolutionary code (Straniero et al. 1995, 1997, 2001). The *s*-process nucleosynthesis calculations were performed with a post-process code and were extended over a wide range of metallicities. Specifically, we make use here of the models for 1.5 and 5 M_{\odot} stars, in order to show how different predictions about abundances and abundance ratios at the Sr-Y-Zr peak that can be obtained when the initial mass is assumed

to belong to the LMS or to the IMS range. Reimer’s (1975) parameterization for mass loss was adopted ($\eta = 0.7$ and 10 , for the $1.5 M_{\odot}$ and the $5 M_{\odot}$ cases, respectively). When models are run at nearly solar metallicity, the one relevant for most of our sample stars, third dredge-up is found to start after a few thermal pulses. The parameter λ (defined as $\Delta M(\text{TDU})/\Delta M_{\text{H}}$, where $\Delta M(\text{TDU})$ is the mass dredged-up in one mixing episode and ΔM_{H} is the extension in mass by which the H shell advances in an interpulse period) is on average 0.24 and 0.38 in the two cases. TDU is followed in detail pulse after pulse, mixing with the envelope material from the He intershell rich in ^{12}C and s -elements. In this way we can follow the stellar envelope composition evolving in time while the star ascends the TP-AGB phase.

The activation of the ^{13}C neutron source requires some protons from the envelope to penetrate into the He intershell when TDU is established. Subsequently, proton captures on the abundant ^{12}C allow the formation of a small ^{13}C -pocket in the uppermost layers of the He intershell. All ^{13}C nuclei are then consumed by α -captures during the interpulse phase, while the intershell zone is in radiative conditions (Straniero et al. 1997). Successful models of the ^{13}C -pocket formation have been presented in the recent years, as a consequence of the application of diffusive or hydrodynamical simulations of the partial mixing occurring at the H-C interface (Iben & Renzini 1982; Hollowell & Iben 1988; Herwig et al. 1997; Cristallo et al. 2001). A general consensus is emerging that such partial mixing events do indeed occur: they might be stimulated by rotational shear (Langer et al. 1999). However, the above models are still very speculative and cannot be used to make general predictions suitable to perform a comparison with observations. Therefore, the amount of ^{13}C in the pocket and the distribution within it must still be considered as free parameters. Following the approach by Busso et al. (2001), we chose here to adopt a wide range of ^{13}C production in the pocket. We start from the reference choices made in Gallino et al. (1998) for LMS, and in Travaglio et al. (2001) for IMS: both choices were called *standard* (ST) in the

original papers. They correspond to a total ^{13}C mass of $4 \times 10^{-6} M_{\odot}$ in LMS and of $4 \times 10^{-7} M_{\odot}$ in IMS. The decrease by an order of magnitude of the strength of the ^{13}C neutron source in the pocket corresponds to the overall decrease by the same order of the mass of the He intershell, the TDU efficiency, and the interpulse period. Then we scale such abundances upward and downward, obtaining cases with efficiencies from a factor of two higher (ST \times 2) to a factor of 12 lower (ST/12).

The envelope composition is progressively enriched by TDU in C and *s*-elements, reaching the condition for a C(N) star ($\text{C/O} > 1$) in the last TPs. For AGB stars of initial mass $1.5 M_{\odot}$ this occurs for any metallicity up to $[\text{Fe}/\text{H}] = +0.2$. Table 5 shows the predicted C/O and $^{12}\text{C}/^{13}\text{C}$ ratios in the envelope after the last TDU episodes where the condition $\text{C/O} > 1$ is met for AGB models of 1.5, 3 and $5 M_{\odot}$ and for the three metallicities $[\text{Fe}/\text{H}] = +0.2, 0.0$ and -0.3 . For each mass, in the third column we also report the remaining envelope mass at the given TP. With the adopted mass loss prescriptions, at $[\text{Fe}/\text{H}] = +0.2$ we do not find $\text{C/O} > 1$ in the envelope of AGB stars of 3 and $5 M_{\odot}$, although we are not far from reaching this condition. Our sample stars span a range -0.3 to $+0.3$ in $[\text{Fe}/\text{H}]$, but the estimated uncertainty of the metallicity and, even more, the observational uncertainty in the mass loss rate does not allow us to make a more detailed analysis such as, for example, to exclude on that all stars with nominal $[\text{Fe}/\text{H}]$ higher than solar are of initial mass below $3 M_{\odot}$.

6. Discussion

6.1. The neutron density and the mass of C stars

Figures 1 and 2 show the run of observed abundance ratios $[\text{X}/\text{M}]$, for Rb, Sr, Y and Zr, compared with AGB model predictions for stars of initial mass 1.5 and $5 M_{\odot}$ and

different metallicities. The plotted curves pick up the envelope composition when the photospheric C/O ratio reaches unity, because we must fulfill the general requirement that our stars are carbon rich with C/O ratios in the range 1.01 to 1.20. The *s*-element abundance predictions for AGB stars of $M = 3 M_{\odot}$ are almost identical to the $M = 1.5 M_{\odot}$ case. An exception is [Rb/Fe], which is 0.1 dex higher for all choices of the ^{13}C -pocket. Different mass loss prescriptions or details on TDU pulse after pulse would not affect much the results, provided C/O = 1 is reached in the envelope.

Table 6 gives the Rb, Sr, Y, and Zr expectations at C/O =1 for the various AGB models and different ^{13}C -pocket prescriptions. All sample stars are reproduced by our theoretical models in the range ST/1.5 to ST/3. Figures 1 and 2 show only a weak tendency of the curves to be non-monotonic versus [M/H] in the range of the bona fide observed C(N) stars. For the $5 M_{\odot}$ model a decrease in *s*-element abundances with decreasing metallicity appears. This predicted trend of envelope abundances is quite different from what has recently been shown in Busso et al. (2001) for the same AGB stellar models, where in particular a steep increase of [ls/Fe] resulted with decreasing [Fe/H], up to a maximum at around +1.2, (which is reached at [Fe/H] ~ -0.5 for the ST case), followed by a decrease at lower metallicities. The discrepancy is only apparent and deals with the particular constraint to be met here, i.e. with the mentioned fact that in our sample C(N) stars, C/O is close to 1 (see Table 1). The trends shown in Busso et al. (2001) are instead representative of the last occurrence of TDU in the models. For a $1.5 M_{\odot}$ star, in our calculations this corresponds to the 17th TDU episode; for solar metallicity this implies C/O = 1.44.

In AGB stars of lower metallicity, given that the ^{12}C production in the top layer of the He intershell is always close to 0.2 in mass fraction, the carbon enrichment in the envelope is more easily established. Therefore the envelope C/O ratio increases steadily

with decreasing metallicity, and is moderated only by the fact that at low $[\text{Fe}/\text{H}]$ the stars condense from an O-enhanced interstellar medium (Wheeler, Sneden & Truran 1989). At $[\text{Fe}/\text{H}] = -1.3$ (close to the estimated metallicity of V CrB) in a $1.5 M_{\odot}$ model after 17 TDUs, $\text{C}/\text{O} = 11.4$ and $^{12}\text{C}/^{13}\text{C} = 2221$. For such a metallicity, a C/O ratio close to unity is found at the very early occurrence of TDU (with a corresponding $^{12}\text{C}/^{13}\text{C} = 135$), when the *s*-process abundances have been barely affected by neutron captures in the He intershell. We underline that this finding should be considered as a general rule for C(N) stars, as observations always reveal a moderate C enrichment. This may imply some selection effect: intrinsic AGB C-stars with higher C/O ratios should exist, as high values of C/O have been observed in both post-AGB stars reaching the pre-planetary nebula stage (Reddy, Bakker, & Hrivnak 1999) and in extrinsic C-rich objects originated by mass transfer phenomena (Vanture 1992c). However, an excess of carbon is immediately translated into a copious production of carbon-rich dust and into a high opacity of the circumstellar environment, to the point of hiding the photosphere at optical wavelengths. This is the case of some infrared carbon stars observed by IRAS (van Loon et al. 1998; Marengo et al. 1999). Therefore, unlike MS-S giants or the extrinsic Ba stars, which display different levels of C enrichment, the *visible* C(N) stars represent a sort of snapshot taken at a particular moment during the TP-AGB evolution, always representing the first appearance of a carbon-rich composition.

Figures 1 and 2 show, however, that non-negligible differences in the *s*-process predictions at $\text{C}/\text{O} = 1$ from a LMS and from an IMS exist. The IMS models show a considerably narrower strip of predicted abundances when the amount of ^{13}C burnt in the pocket is varied as compared with the LMS case. This is true especially for $[\text{Rb}/\text{Fe}]$. These IMS predictions, as a whole, seem scarcely compatible with most sample stars.

In Figures 3 and 4 we plot the elemental ratios $[\text{Rb}/\text{Sr}]$, $[\text{Rb}/\text{Y}]$ and $[\text{Rb}/\text{Zr}]$ versus metallicity. Of the three panels in the figures, the one yielding the clearest distinction

is the second one, [Rb/Y]. According to the discussion of § 2, the fact that IMS models (where the ^{22}Ne source is active) compare less favourably with the data is an indication that most neutron fluxes at the origin of the observed s -element enhancements come from the ^{13}C source, and consequently that most C(N) stars are of low initial mass.

Eventually, in Figure 5 we use [ls/M] as the average abundance of [Y/M] and [Zr/M], after excluding Sr, whose abundance is more uncertain. The entire sample of stars having a measurement for the three elements: Rb, Y and Zr, are (with the exception of IY Hya) compatible with a metallicity $[M/H] = 0.0 \pm 0.30$ and actually fulfills this requirement within 1σ . Figure 5 considers only model sequences above $[\text{Fe}/\text{H}] = -0.3$. Along the theoretical curves, the predicted [Rb/Y] increases with increasing [Fe/H]; exception is the ST case for $M = 1.5 M_{\odot}$, for which the lower [Fe/H] corresponds to the lower [ls/Fe]. The plot immediately displays the characteristics discussed above: LMS models occupy the region of negative [Rb/Y], IMS models stay on the opposite side, and the partial overlapping of figures 1 and 2 is avoided.

6.2. Carbon isotopes and related problems

Figure 6 shows in graphic form the C/O observed ratio versus $^{12}\text{C}/^{13}\text{C}$. Current stellar models yield a small reduction in C/O (by 30 %) and a consistent reduction of the $^{12}\text{C}/^{13}\text{C}$ ratio (by a factor 4) during the first ascent of the red giant branch, caused by the first dredge up mechanism (FDU). The reduction by a factor of 4 from the solar ratio ($^{12}\text{C}/^{13}\text{C} = 89$) is obtained after decreasing by one third of the initial ^{12}C abundance and through an increase by a factor ~ 2.5 of ^{13}C , both changes being due to proton captures on ^{12}C during the main sequence in the deep regions of the radiative H-rich envelope (e.g., Dearborn 1992). Note that the resulting ratio after the FDU is independent of the initial $^{12}\text{C}/^{13}\text{C}$ value. The same FDU results are obtained for different initial metallicities, even

when one accounts for the fact that, in Galactic evolution, $N(^{12}\text{C})$ scales as $N(\text{Fe})$, while $N(^{13}\text{C})$ scales as $N(\text{Fe})^2$ (Iben 1977; Boothroyd & Sackmann 1988).

However, at least for masses smaller than about $2 M_{\odot}$ the canonical reduction of the $^{12}\text{C}/^{13}\text{C}$ ratio at FDU down to 20 – 25 is insufficient to explain the observations in red giants (Gilroy & Brown 1991; Charbonnel, Brown, & Wallerstein 1998; Gratton et al. 2000). A similar discrepancy with model predictions is shown by oxygen and carbon isotopes measured in dust grains of clear AGB circumstellar origin, recovered from meteorites. This is true both for C-rich (Anders & Zinner 1993) and for O-rich grains (Nittler et al. 1994; Hutcheon et al. 1994). Explanation of this evidence involves a relatively slow process of mixing occurring during the RGB in the radiative region located between the bottom of the convective envelope and the H-burning shell, perhaps induced by rotation (Sweigart & Mengel 1979). This process is sometimes called Cool Bottom Process, or CBP (Wasserburg, Boothroyd, & Sackmann 1995). CBP has been shown to yield quite naturally enhancements of ^{13}C and of ^{17}O and reductions in ^{18}O . Several phenomenological models have been presented for such phenomena (Boothroyd, Sackmann, & Wasserburg 1994; Denissenkov & Weiss 1996; Weiss, Denissenkov, & Charbonnel 2000). The general agreement with observations has led to acceptance that such circulations should indeed be active, thus further reducing in LMS red giants the $^{12}\text{C}/^{13}\text{C}$ ratio established after the FDU. The exact extent of the depletion as a function of mass for each metallicity is, to date, rather uncertain, as the requirement of sampling low mass objects has often led to obtain the measurements in metal poor clusters, so that the two parameters (mass and metal content) are coupled and difficult to separate. Recently, Charbonnel, Brown, & Wallerstein (1998) have started a project on field stars whose parallax was accurately measured by HIPPARCOS, and a clearer view is now emerging, in which giant stars of the old Galactic disc population (at metallicities $[\text{Fe}/\text{H}] \sim -0.6$) can reach $^{12}\text{C}/^{13}\text{C}$ ratios close to 7. For more metal-rich stars a reasonable estimate might be 10 – 15 (Gilroy & Brown 1991). Not

having a suitable model for CBP, we chose this estimate as the $^{12}\text{C}/^{13}\text{C}$ ratio present in early AGB phases of LMS before the onset of thermal pulses: the adopted tentative value is 12. For stars more massive than $\sim 2.5 M_{\odot}$, we assumed $^{12}\text{C}/^{13}\text{C} = 24$.

When we then add ^{12}C to the envelope by TDUs along the AGB, the isotopic ratio raises. At $\text{C}/\text{O} \sim 1$ a pre-AGB value of around 25 would translate into a final value a bit higher than the solar isotopic ratio ($^{12}\text{C}/^{13}\text{C}=89$). Indeed, after a few TPs, when TDU is operating, a nearly constant mass fraction of ^{12}C , $X(^{12}\text{C}) \sim 0.23$, is built in the He intershell by partial He burning in the TP. This is independent of the core mass, i.e. on the AGB initial mass. About identical results are obtained by different authors (see e.g., Iben 1976, 1982; Boothroyd & Sackmann 1988; Straniero et al. 1995, 1997; Mowlavi 1999). Only a marginal production of ^{16}O occurs in the TP, so that the oxygen abundance in the envelope is not affected by TDU. Also the ^{13}C abundance in the envelope is not affected by TDU, since no ^{13}C nuclei are left in the He intershell, while the mass of the He intershell cumulatively mixed with the surface is a small fraction of the envelope. Under those conditions, it is easy to evaluate the $^{12}\text{C}/^{13}\text{C}$ in the envelope at $\text{C}/\text{O} = 1$. It results: $^{12}\text{C}/^{13}\text{C} \sim 3.6 \times (^{12}\text{C}/^{13}\text{C})_{\text{FDU}}$. This relation is independent of metallicity if both ^{12}C and ^{16}O are assumed to scale as Fe. Actually, for $[\text{Fe}/\text{H}] = -0.3$ we introduced a modest α -enhancement in the initial ^{16}O abundance with respect to a solar-scaled metallicity composition, according to an average observational trend $[\text{O}/\text{Fe}] = -0.5 [\text{Fe}/\text{H}]$ (cf. Wheeler, Sneden, & Truran 1989). This implies an increase by about 30% of the predicted $^{12}\text{C}/^{13}\text{C}$ ratio at $\text{C}/\text{O} = 1$.

As shown in figure 6, only two stars, V Aql and W Ori, show the expected ratio at $\text{C}/\text{O} \sim 1$, without requiring any CBP to operate. Those two stars should have a mass higher than $2.5 M_{\odot}$, perhaps around $3 M_{\odot}$. When we consider the majority of our sample stars, which have previously been shown to be of low mass, we immediately see that CBP must

have reduced the $^{12}\text{C}/^{13}\text{C}$ ratio. Actually, even a CBP operating only on the RGB would be insufficient, as according to the previously given rule, starting from $(^{12}\text{C}/^{13}\text{C})_{\text{FDU}} \sim 12$ we would have final values of 43 (see Figure 6). Hence CBP should be active also later, in the early AGB phase, to operate changes larger than we assumed and thus explain the later part of the $^{12}\text{C}/^{13}\text{C}$ distribution. The possibility exists that CBP operates also in the TP-AGB phase, though calculations have not been performed yet. A different efficiency of rotationally induced meridional mixing (Sweigart & Mengel 1979) in different stars might also accomplish this job.

Furthermore, in the above discussion we assumed that all sample stars are intrinsic AGBs. This actually may not be true. A considerable fraction of C(N) stars might be extrinsic AGBs belonging to binary systems (see § 4.1). In this case, the observed star could be ascending the early AGB phase, having being enriched in carbon and *s*-process elements by mass transfer from the more massive companion while this last was on the AGB. In this case FDU on the companion star can further reduce the $^{12}\text{C}/^{13}\text{C}$ ratio ⁸.

7. Conclusions

In this paper we have presented new high-resolution spectroscopic measurements for carbon-rich AGB stars belonging to the C(N) type. We have focused our attention on *s*-elements around the ^{85}Kr reaction branching of the *s*-process path, showing that the comparative analysis of Rb, Sr, Y, and Zr yields information on the neutron density prevailing during the neutron capture nucleosynthesis processes occurring in the He

⁸Note, that actually there is a controversy on the typical $^{12}\text{C}/^{13}\text{C}$ ratio in C(N)-stars (see Lambert et al. 1986; Ohnaka & Tsuji 1996-98; de Laverny & Gustafsson 1998-99; Schöier & Olofsson 2000).

intershell. Despite the large uncertainty existing in the derivation of element abundances in these stars, comparison with AGB nucleosynthesis models, which were already capable of explaining the abundances in other intrinsic and extrinsic classes of AGB stars, confirms a general agreement between theoretically predicted photospheric compositions and observations. The main implication of such an analysis is that most C(N) stars are of low mass, experiencing *s*-process nucleosynthesis phenomena dominated by the neutron source provided by α captures on ^{13}C in radiative intershell layers. When the $^{12}\text{C}/^{13}\text{C}$ ratios are considered, their generally low values require the activation of slow circulation mechanisms below the formal convective border of the envelope, bringing material close to the H-burning shell and therefore increasing the abundance of ^{13}C . These mechanisms are indeed known to occur in stars below about $2 M_{\odot}$: this implies, therefore, the conclusion that the majority of C(N) stars are of small mass. Exceptions might exist in a very few cases, though this speculation is highly uncertain and should be verified by more extensive measurements of *s*-process elements, especially at the Ba-peak.

We thank the referee for the very careful reading of the manuscript and his valuable comments and suggestions. C. Abia is grateful to P. de Laverny and B. Plez for providing the CN and C₂ line lists in the wavelength ranges studied. Data from the VALD database at Vienna were used for the preparation of this paper. K. Eriksson, and the stellar atmosphere group of the Uppsala Observatory are thanked for providing the grid of atmospheres. The 4.2m WHT is operated on the island of La Palma by the RGO in the Spanish Observatory del Roque de los Muchachos of the Instituto de Astrofísica de Canarias. This work was also based in part on observations collected at the German-Spanish Astronomical Centre, Calar Alto, Spain. It was partially supported by grants PB96-1428, ESP98-1348 and AYA2000-1574, by the Italy-Spain agreement HI1998-0095 and by the Italian MURST-Cofin2000 project ‘Stellar Observables of Cosmological Relevance’.

REFERENCES

- Abia, C., & Isern, J. 1996, *ApJ*, 460, 443
- Abia, C., & Isern, J. 1997, *MNRAS*, 289, L11
- Abia, C., & Isern, J. 2000, *ApJ*, 449, 438 (Paper II)
- Abia, C., Pavlenko, Ya., & de Laverny, P. 1999, *A&A*, 351, 273
- Abia, C., & Wallerstein, G. 1998, *MNRAS*, 293, 89 (Paper I)
- Allen, C.W. 1976, *Astrophysical Quantities*, The Athlone Press
- Anders, E., & Grevesse, N. 1989, *Geochim. Cosmochim. Acta*, 53, 197
- Anders, E., & Zinner, E. 1993, *Meteoritics*, 28, 490
- Barnbaum, C., Stone, R.P.S., & Keenan, P.C. 1996, *ApJS*, 105, 419
- Beer, H., & Macklin, R. L. 1989, *ApJ*, 339, 962
- Blöcker, T., & Schönberner, D. 1991, *A&A*, 244, L43
- Biémont, E., Grevesse, N., Hannaford, P., & Lowe, R.M. 1981, *ApJ*, 248, 867
- Boothroyd, A.I, & Sackmann, I. 1988, *ApJ*, 328, 653
- Boothroyd, A.I, & Sackmann, I. 1992, *ApJ*, 393, L21
- Boothroyd, A.I, Sackmann, I., & Ahern, C. 1993, *ApJ*, 416
- Boothroyd, A.I, Sackmann, I.-J., & Wasserburg, G.J. 1994, *ApJ*, 430, L77
- Busso, M., Gallino, R., & Wasserburg, G.J. 1999, *ARA&A*, 37, 239
- Busso, M., Lambert, D.L., Gallino, R., Travaglio, C., & Smith, V.V. 2001, *ApJ*, in press

- Charbonnel, C., Brown, J.A., & Wallerstein, G. 1998, *A&A*, 332, 204
- Claussen, M.J., Kleinmann, S.G., Joyce, R.R., & Jura, M. 1987, *ApJS*, 65, 385
- Cristallo, S., Gallino, R., Straniero, O., Lugaro, M., & Busso, M. 2001, *Nucl. Phys. A*, in press
- Corliss, C.H., & Bozman, W.R. 1962, *NBS Monograph* 53
- Dearborn, D. S. P. 1992, *Phys. Rep.*, 210, 367
- de Laverny, P., & Gustafsson, B. 1998, *A&A*, 332, 661
- de Laverny, P., & Gustafsson, B. 1999, *A&A*, 346, 520
- Denissenkov, P. A., & Weiss, W.W. 1996, *A&A*, 308, 773
- Dyck, H.M., van Belle, G.T., & Benson, J.A. 1996, *AJ*, 112, 96
- Eriksson, K., Gustafsson, B., Jørgensen, U., & Nordlund, A. 1984, *A&A*, 132, 37
- Forestini, M., & Charbonnel, C. 1996, *A&AS*, 123, 241
- Fouqué, P., Le Bertre, T., Epchtein, N., Guglielmo, F., & Kerschbaum, F. 1992, *A&A*, 93, 151
- Frogel, J.A., Mould, J., & Blanco, V.M. 1990, *ApJ*, 352, 96
- Frost, C.A., Cannon, R.C., Lattanzio, J.C., Wood, P.R., & Forestini, M. 1998, *A&A*, 332, L17
- Fuhr, J.R., Martin, G.A., & Wiese, W.L. 1988, *J.Phys.Chem.Ref.Data* 17, Suppl. 4
- Gallino, R., Arlandini, C., Busso, M., Lugaro, M., Travaglio, C., Straniero, O., Chieffi, A., & Limongi, M. 1998, *ApJ*, 497, 388

- Gilroy, K., & Brown, J.A. 1991, *ApJ*, 371, 578
- Gratton, R., Sneden, C., Carretta, E., & Bragaglia, A. 2000, *A&A*, 354, 169
- Groenewegen, M.A.T., Whitelock, P.A., Smith, C.H., & Kerschbaum, F. 1998, *MNRAS*, 293, 18
- Hannaford, P., Lowe, R.M., Grevesee, N., Biémont, E., & Whaling, W. 1982, *ApJ*, 261, 736
- Herwig, F. 2000, *A&A*, 360, 952
- Herwig, F., Blöcker, T., Schönberner, D., & El Eid, M. 1997, *A&A*, 324, L81
- Hollowell, D.E., & Iben, I. Jr. 1988, *ApJ*, 333, L25
- Holweger, H., & Müller, E.A. 1974, *Sol. Phys.*, 39, 19
- Hughes, S.M., & Wood, P.R. 1990, *AJ*, 99, 784
- Hutcheon, I.D., Huss, G.R., Fahey, A.J., & Wasserburg, G.J. 1994, *ApJ*, 425, L97
- Iben, I. Jr. 1975, *ApJ*, 196, 525
- Iben, I. Jr. 1976, *ApJ*, 208, 165
- Iben, I. Jr. 1977, in *Advanced Stages of Evolution*, eds. I. Iben Jr., A. Renzini, & D.N. Schramm, (Sauverny: Geneva Observatory), 1
- Iben, I. Jr 1981, *ApJ*, 246, 278
- Iben, I. Jr 1982, *ApJ*, 260, 821
- Iben, I. Jr., & Truran, J.W. 1978, *ApJ*, 220, 980
- Iben, I. Jr, & Renzini, A. 1982, *ApJ*, 263, L23

- Iben, I. Jr, & Renzini, A. 1983, *ARA&A*, 21, 271
- Jorissen, A., Frayer, D.T., Johnson, H.R., Mayor, M., & Smith, V.V. 1993, *A&A*, 271, 463
- Jura, M., & Kleinmann, S.G. 1989, *ApJ*, 341, 359
- Käppeler, F., Beer, H., & Wisshak, K. 1989, *Rep. Prog. Phys.*, 52, 945
- Keenan, P.C., & Boeshaar, P.C. 1980, *ApJS*, 43, 379
- Kipper, T. 1998, *Baltic Astronomy A*, 7, 435
- Komarovskij, V.A., 1991, *Opt. & Spectroskopia* 71, 559
- Lambert, D.L., Gustafsson, B., Eriksson, K., & Hinkle, K. H. 1986, *ApJS*, 62, 373
- Lambert, D.L., Smith, V.V., Busso, M., Gallino, R., & Straniero, O. 1995, *ApJ*, 450, 302
- Langer, N., Heger, A., Wellstein, S., & Herwig, F. 1999, *A&A*, 346, 37
- Lattanzio, J.C. 1989, *ApJ*, 344, L25
- Lattanzio, J.C., & Forestini, M. 1998, in *Asymptotic Giant Branch Stars*, IAU Symp. 191, eds. T. Le Bertre, A. Lèbre, & C. Waelkens, (San Francisco: ASP), 31
- Lattanzio, J. C., Frost, C., Cannon, R., & Wood, P.R., 1996, *Mem. Soc. Astron. It.*, 67, 729
- Little, S.J., Little-Marenin, I.R., & Hagen, W. 1987, *AJ*, 94, 981
- Malaney, R.A., & Lambert, D.L. 1988, *MNRAS*, 235, 695
- Marengo, M., Busso, M., Persi, P., Silvestro, G., & Lagage, P.O. 1999, *A&A*, 348, 501
- Martin, G.A., Fuhr, J.R., & Wiese, W.L. 1988, *J.Phys.Chem.Ref.Data* 17, Suppl. 3
- Merrill, P.W. 1952, *ApJ*, 321, 832

- Moore, C.E., Minnaert, M.G.J., & Hootgast, J. 1996, *The Solar Spectrum, 2935 Å to 8770 Å*, NBS Monog. No. 61 NBS, Washington, DC.
- Mowlavi, N. 1999, *A&A*, 344, 617
- Neugebauer, G., & Leighton, R.B. 1969, *Two-Micron Sky Survey*, NASA SP-3047(TMSS)
- Nittler, L.R., Alexander, C.M.O.D., Gao, X., Walker, R.M., & Zinner, E. 1994, *Nature*, 370, 443
- Noguchi, K., Kawara, K., Kobayashi, K., Okuda, H., Sato, S., & Oishi, M. 1981, *PASJ*, 33, 373
- Ohnaka, K., & Tsuji, T. 1996, *A&A*, 310, 933
- Ohnaka, K., & Tsuji, T. 1998, *A&A*, 335, 1018
- Piskunov, N.E., Kupka, F., Ryabchikove, T.A., Weiss, W.W., & Jeffry, C.S. 1995, *A&AS*, 285, 541
- Plez, B. 1999, in *Asymptotic Giant Branch Stars*, IAU Symp. 191, eds. T. Le Bertre, A. Lèbre, & C. Waelkens, (San Francisco: ASP), 75
- Plez, B., Smith, V.V., & Lambert, D.L. 1993, *ApJ*, 418, 812
- Reddy, B.E., Bakker, E.J, & Hrivnak, B.J. 1999, *ApJ*, 524, 831
- Reimers, D. 1975, in *Stellar Atmospheres and Envelopes*, eds. B. Bashek, H. Kegel, & G. Traving, (Berlin: Springer), 229
- Schöier, F. L., & Olofsson, H. 2000, *A&A*, astrph-0005360
- Smith, V.V., Cunha, K., Jorissen, A., & Boffin, H.M.J. 1997, *A&A*, 324, 97
- Smith, V.V., & Lambert, D.L. 1985, *ApJ*, 294, 326

- Smith, V.V., & Lambert, D.L. 1986, *ApJ*, 311, 843
- Smith, V.V., & Lambert, D.L. 1988, *ApJ*, 333, 219
- Smith, V.V., & Lambert, D.L. 1990, *ApJS*, 72, 387
- Smith, V.V., Suntzeff, N.B., Cunha, K., Gallino, R., Busso, M., Lambert, D.L., & Straniero, O. 2000, *AJ*, 119, 1239
- Straniero, O., Chieffi, A., Limongi, M., Busso, M., Gallino, R., & Arlandini, C. 1997, *ApJ*, 478, 332
- Straniero, O., Gallino, R., Busso, M., Chieffi, A., Raiteri, C., Salaris, M., & Limongi, M. 1995, *ApJ*, 440, L85
- Straniero, O., Limongi, M., Chieffi, A., Domínguez, I., Busso, M., & Gallino, R. 2001, in *Changes in the Abundances of AGB Stars*, eds. F. D'Antona & R. Gallino, *Mem. Soc. Astron. It.*, in press
- Sugimoto, D. 1971, *Progr. Theor. Phys.*, 45, 761
- Sweigart, A.V., & Mengel, J.G. 1979, *ApJ*, 229, 624
- Takeda, Y., Kato, K.I., Watanabe, Y., & Sadakane, K. 1996, *PASJ*, 48, 511
- Thévenin, F. 1989, *A&AS*, 77, 137
- Thévenin, F. 1990, *A&AS*, 82, 179
- Tomkin, J., & Lambert, D.L. 1983, *ApJ*, 273, 722
- Tomkin, J., & Lambert, D.L. 1999, *ApJ*, 523, 234

- Trams, N.R., van Loon, J.Th., Zijlstra, A.A., Loup, C., Groenewegen, M.A.T., Waters, L.B.F.M., Whitelock, P.A., Blommaert, J.A.D.L., Siebenmorgen, R., & Heske, A. 1999, *A&A*, 344, L17
- Travaglio, C., Gallino, R., Busso, M., & Gratton, R.G. 2001, *ApJ*, 549, 346
- Utsumi, K. 1970, *PASJ*, 22, 93
- Utsumi, K. 1985, in *Cool Stars with Excesses of Heavy Elements*, eds. M. Jascheck & P.C. Keenan (Dordrecht: Reidel), 243
- Vaglio, P., Gallino, R., Busso, M., Travaglio, C., Straniero, O., Chieffi, A., Limongi, M., Lugaro, M., Arlandini, C. 1999, in *Nuclei in the Cosmos V*, eds. N. Prantzos & S. Harissopulos, (Paris: Editions Frontières), 223
- van Loon, J.T.H., Zijlstra, A.A., & Groenewegen, M.A.T. 1999, *A&A*, 346, 805
- van Loon, J.T.H., Zijlstra, A.A., Whitelock, P.A., te Lintel Hekkert P., Chapman, J.M., Loup, C. 1998, *A&A*, 329, 169
- Vanture, A.D. 1992a, *AJ*, 103, 2035
- Vanture, A.D. 1992b, *AJ*, 104, 1997
- Vanture, A.D. 1992c, *AJ*, 104, 1986
- Vanture, A.D., Wallerstein G., & Brown, J.A. 1994, *PASP*, 106, 835
- Wallerstein, G., et al. 1997, *Rev. Mod. Phys.*, 69, 4
- Wallerstein, G., & Knapp, G.R. 1998, *ARA&A*, 36, 369
- Wasserburg, G.J., Boothroyd, A.I., & Sackmann, I.-J. 1995, *ApJ*, 440, L101
- Weiss, A., Denissenkov, P.A., & Charbonnel, C. 2000, *A&A*, 356, 181

Wheeler, J.C., Sneden, C., & Truran, J. 1989, *ARA&A*, 27, 279

Wiese, W.L., & Fuhr, J.R. 1975, *J.Phys.Chem.Ref.Data* 4, 263

Table 1. Data for Program Stars

Star	Spec. Type	T_{eff}	Ref. ^a	C/O	$^{12}\text{C}/^{13}\text{C}$	Ref. ^b
AQ And	C5,4	2970*	2	1.02	30	1
AW Cyg	C3,6	2760	2	1.03	21	2
EL Aur	C5,4	3000	6	1.07	50	2
HK Lyr	C6,4	2866	2	1.02	10	2
IRC –10397	N	2600	6	1.01	20	2
IY Hya	N	2500	6	1.02	15	2
LQ Cyg	C4,5	2620	2	1.10	40	2
RX Sct	C5,2	3250	2	1.04	60	2
S Sct	C6,4	2895	1	1.07	45	3
SY Per	C6,4	3070	3	1.02	43	2
SZ Sgr	C7,3	2480	2	1.03	8	2
TY Oph	C5,5	2780*	2	1.05	45	2
U Cam	C3,9	2670	2	1.02	40	2
UU Aur	C5,3	2825	1	1.06	50	3
UV Aql	C6,2	2750	2	1.005	19	2
UX Dra	C7,3	2900	1	1.05	26	2
V Aql	C6,4	2610	1	1.16	90	2
V CrB	C6,2	2250	4	1.10	10	4
V Oph	C5,2	2880*	2	1.05	11	1
VX Gem	C7,2	2500	5	1.01	60	2

Table 1—Continued

Star	Spec. Type	T_{eff}	Ref. ^a	C/O	$^{12}\text{C}/^{13}\text{C}$	Ref. ^b
V460 Cyg	C6,3	2845	1	1.06	61	4
V781 Sgr	N	3160	2	1.02	35	3
W Ori	C5,4	2680	1	1.20	79	4
WZ Cas	C9,2J	3140	3	1.005	4	3
Z Psc	C7,2	2870	1	1.01	55	4

^aReferences for T_{eff} : (1) Lambert et al. (1986); (2) Ohnaka & Tsuji (1996); (3) Dyck, van Belle & Benson (1996); (4) Kipper (1998); (5) Groenewegen et al. (1998); (6) For these stars we have estimated the effective temperature by comparing their spectra with the temperature sequence spectral atlas for C-stars created by Barnbaum et al. (1996).

^bSource for the $^{12}\text{C}/^{13}\text{C}$ ratio: (1) Ohnaka & Tsuji (1996); (2) Derived in this work; (3) Lambert et al. (1986); (4) Kipper (1998)

Table 2. Abundances Derived in Program Stars

Star	[M/H]	[Rb/M]	[Sr/M]	[Y/M]	[Zr/M]	Tc
AQ And	0.02	0.3	0.6	0.7	0.5	no
AW Cyg	0.0	0.2	0.4	0.3	0.5	yes
EL Aur	−0.06	0.4	0.5	0.7	0.8	no
HK Lyr	−0.10	0.2	0.3	0.7	0.7	yes
IRC −10397	0.10	0.1	0.3
IY Hya	−0.80	0.5	0.6	0.6	1.0	...
LQ Cyg	0.25	0.2	0.5	0.8	0.7	no
RX Sct	−0.05	0.4	0.4	0.7	0.8	no
S Sct	0.01	0.5	0.8	0.7	0.5	yes
SY Per	−0.30	0.1	0.5	doubf
SZ Sgr	−0.04	0.1	0.4	0.8	0.8	doubf ^a
TY Oph	0.10	0.2	0.6	0.7	0.6	doubf
U Cam	−0.09	0.6	0.4	no
UU Aur	0.06	0.4	0.4	0.6	0.6	no
UV Aql	−0.06	0.6	0.5	0.7	0.9	yes
UX Dra	−0.20	0.0	0.8	0.8	0.8	yes ^a
V Aql	−0.05	0.3	0.5	no
V CrB	−1.35	−0.2	0.3	0.4	...	no ^a
V Oph	0.0	−0.2	0.2	0.3	0.4	...
VX Gem	−0.15	...	0.6	0.5	0.6	yes ^a
V460 Cyg	−0.04	0.4	0.2	0.4	0.4	yes

Table 2—Continued

Star	[M/H]	[Rb/M]	[Sr/M]	[Y/M]	[Zr/M]	Tc
V781 Sgr	0.10	0.1	0.5	0.3	0.2	yes
W Ori	0.05	...	0.0	0.3	0.1	no ^a
Z Psc	−0.01	0.9	0.9	1.0	0.8	yes

^aLittle et al. (1987) classified SZ Sgr as *possible* star showing Tc and reported Tc detection in UX Dra. Kipper (1998) sets an upper limit to the Tc abundance in V CrB ($\log (\text{Tc}/\text{H}) + 12 \lesssim -0.5$) from the analysis of the 5924 Å Tc I line. However, our analysis is compatible with no Tc. For VX Gem and W Ori we were able to get spectra in the 4260 Å region whose analysis confirmed the figure found from the 5924 Å Tc I analysis.

Table 5. C/O and $^{12}\text{C}/^{13}\text{C}$ Predictions in the Envelope

Metallicity	$1.5 M_{\odot}$			$3 M_{\odot}$			$5 M_{\odot}$		
	C/O	$^{12}\text{C}/^{13}\text{C}$	M_{env}	C/O	$^{12}\text{C}/^{13}\text{C}$	M_{env}	C/O	$^{12}\text{C}/^{13}\text{C}$	M_{env}
[Fe/H]= +0.2	1.00	43	0.28
	1.05	45	0.24
[Fe/H]= +0.0	1.06	46	0.38	1.00	91	1.05	1.00	92	1.23
	1.17	51	0.34	1.04	94	0.98	1.04	95	1.16
	1.27	55	0.31	1.08	98	0.91	1.08	99	1.09
	1.37	60	0.28	1.11	101	0.83	1.12	103	1.02
	1.45	63	0.24	1.14	104	0.76	1.16	107	0.95
	1.21	111	0.88
	1.26	116	0.80
	1.32	122	0.73
[Fe/H]= -0.3	1.01	62	0.44	1.01	131	1.31	1.01	132	1.58
	1.16	72	0.41	1.08	140	1.24	1.05	137	1.51
	1.31	81	0.38	1.13	146	1.18	1.09	143	1.44
	1.47	92	0.34	1.18	154	1.11	1.13	149	1.37
	1.61	101	0.31	1.23	160	1.05	1.18	155	1.30
	1.76	110	0.28	1.28	167	0.98	1.23	162	1.23
	1.86	117	0.24	1.34	174	0.91	1.28	169	1.16
	1.38	180	0.83	1.33	176	1.09
	1.44	187	0.76	1.39	184	1.02
	1.45	193	0.95
	1.52	202	0.88
...	1.59	212	0.80	

Table 6. Abundance Ratios at C/O= 1 for different AGB models and ^{13}C -pocket prescriptions

Model	^{13}C -pocket	C/O	$^{12}\text{C}/^{13}\text{C}$	[Rb/Fe]	[Sr/Fe]	[Y/Fe]	[Zr/Fe]
$1.5 M_{\odot}$ [Fe/H]= +0.2	ST	1.00	43	0.51	0.91	0.82	0.70
	ST/1.5	1.00	43	0.31	0.61	0.52	0.39
	ST/3	1.00	43	0.09	0.16	0.10	0.05
$1.5 M_{\odot}$ [Fe/H]= +0.0	ST	1.06	46	0.56	1.06	0.96	0.82
	ST/1.5	1.06	46	0.37	0.75	0.65	0.54
	ST/3	1.06	46	0.12	0.28	0.20	0.12
$1.5 M_{\odot}$ [Fe/H]= -0.3	ST	1.07	46	0.39	1.12	1.12	1.08
	ST/1.5	1.07	46	0.37	0.95	0.86	0.73
	ST/3	1.07	46	0.16	0.46	0.37	0.29
$3 M_{\odot}$ [Fe/H]= +0.0	ST	1.00	91	0.71	1.05	0.98	0.85
	ST/1.5	1.00	91	0.51	0.75	0.68	0.57
	ST/3	1.00	91	0.20	0.29	0.22	0.14
$3 M_{\odot}$ [Fe/H]= -0.3	ST	1.07	97	0.47	1.14	1.15	1.10
	ST/1.5	1.07	97	0.46	0.96	0.89	0.76
	ST/3	1.07	97	0.22	0.48	0.40	0.32
$5 M_{\odot}$ [Fe/H]= +0.0	ST	1.00	92	1.33	1.11	1.08	1.29
	ST/1.5	1.00	92	1.24	0.93	0.87	1.02
	ST/3	1.00	92	1.04	0.71	0.63	0.73
$5 M_{\odot}$ [Fe/H]= -0.3	ST	1.01	93	0.92	0.91	0.96	1.29
	ST/1.5	1.01	93	1.02	0.89	0.89	1.12
	ST/3	1.01	93	0.96	0.67	0.61	0.74

Fig. 1.— Derived abundance ratios $[X/M]$ vs. $[M/H]$ in our sample of C-stars (dots) compared with the corresponding theoretical predictions (lines) for a $1.5 M_{\odot}$ TP-AGB star when the envelope reaches $C/O \gtrsim 1$ for different parameterizations of the ^{13}C pocket (see text). A typical error bar is shown. In the stars where a very few number of lines are used the error bar is certainly larger. Note, furthermore, that the data points for IY Hya, VX Gem and V CrB are plotted with smaller symbols to indicate that the abundance ratios derived in them are very uncertain.

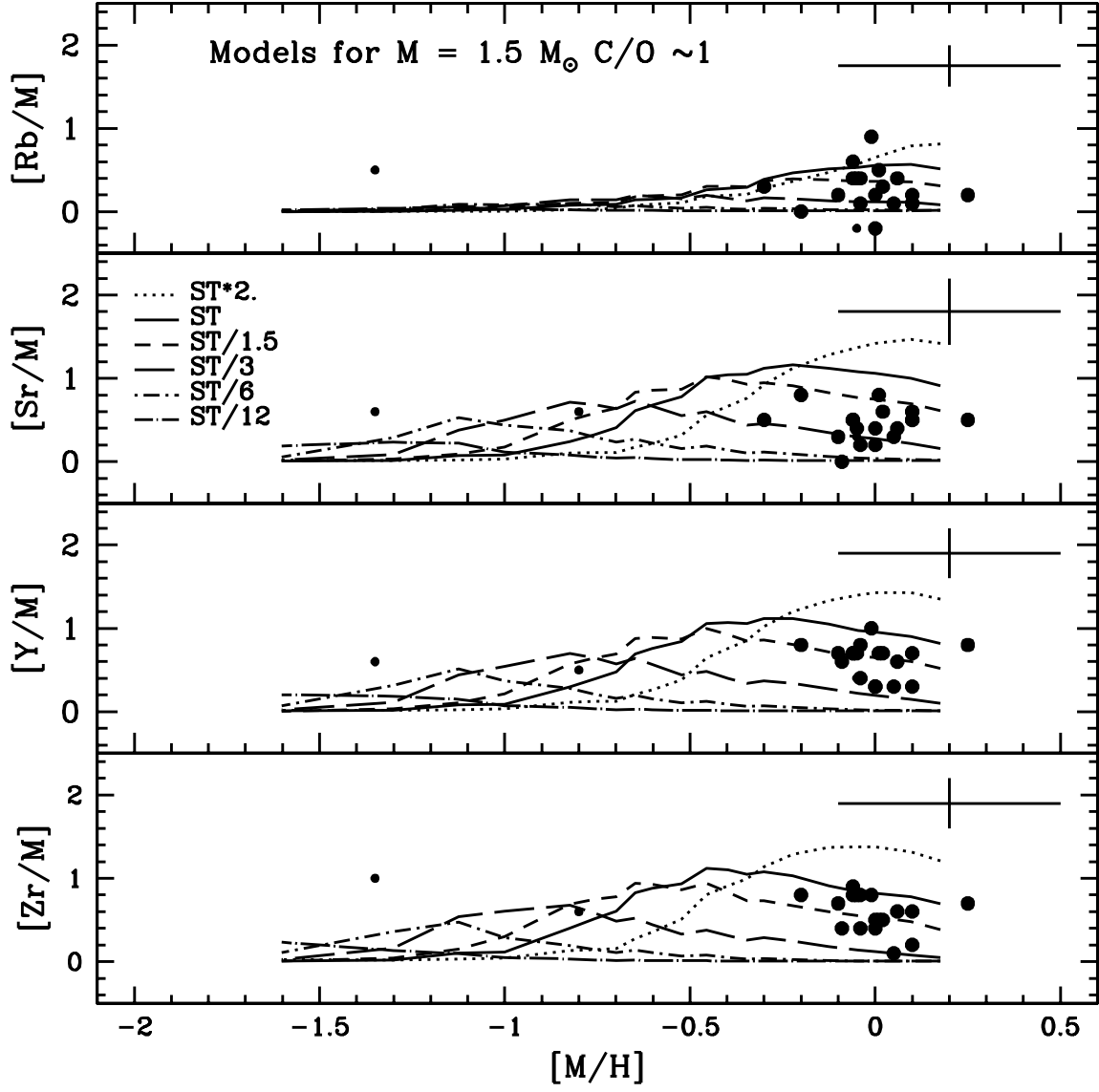
Fig. 2.— As Figure 1 comparing with theoretical predictions for a $5 M_{\odot}$ TP-AGB star.

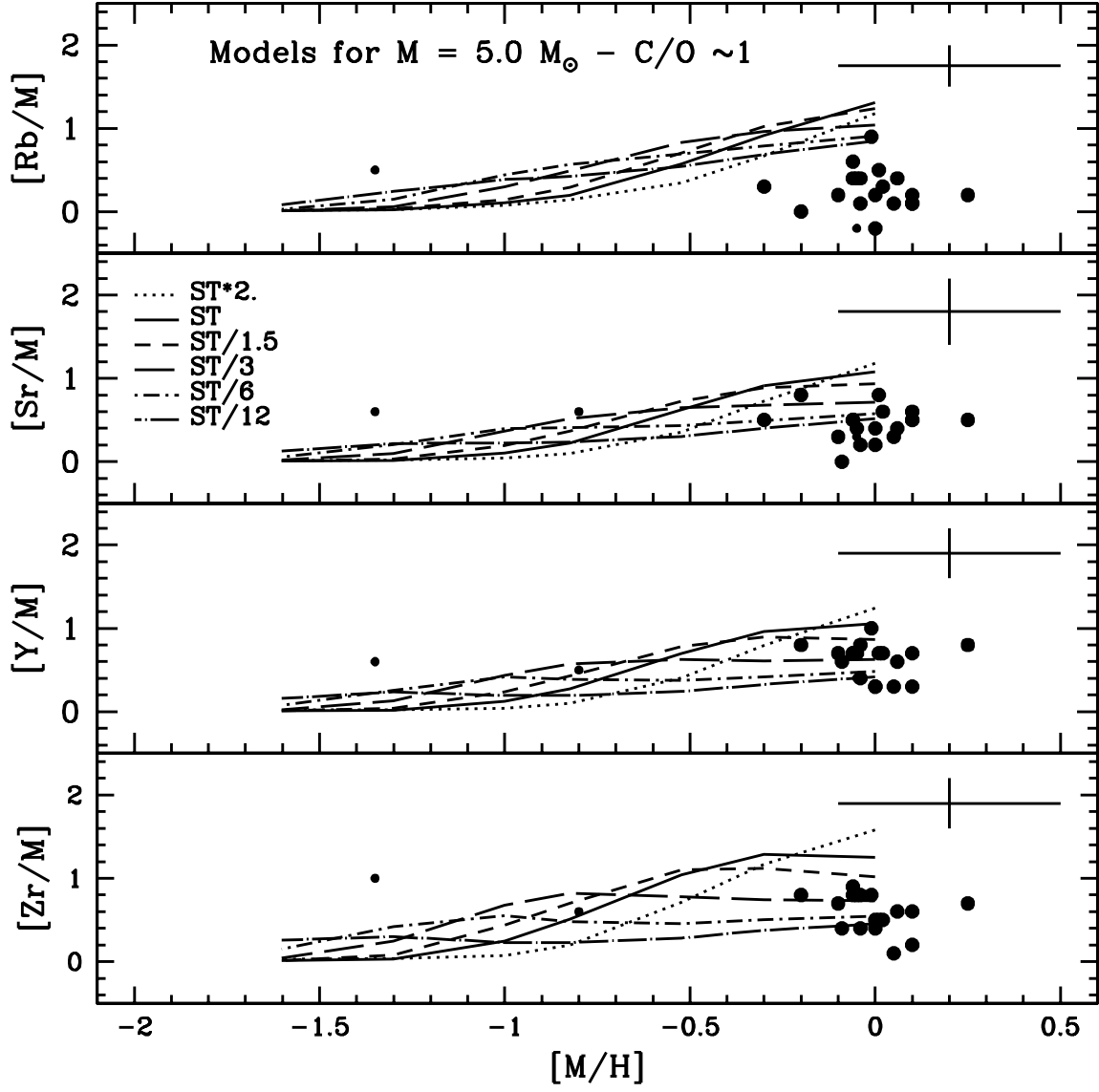
Fig. 3.— Comparison of the observed $[\text{Rb}/\text{Sr}, \text{Y}, \text{Zr}]$ ratios vs. $[M/H]$ with different theoretical predictions for a $1.5 M_{\odot}$ TP-AGB star when the envelope reaches $C/O \gtrsim 1$. Note that again the data points for IY Hya, VX Gem and V CrB are plotted with smaller symbols.

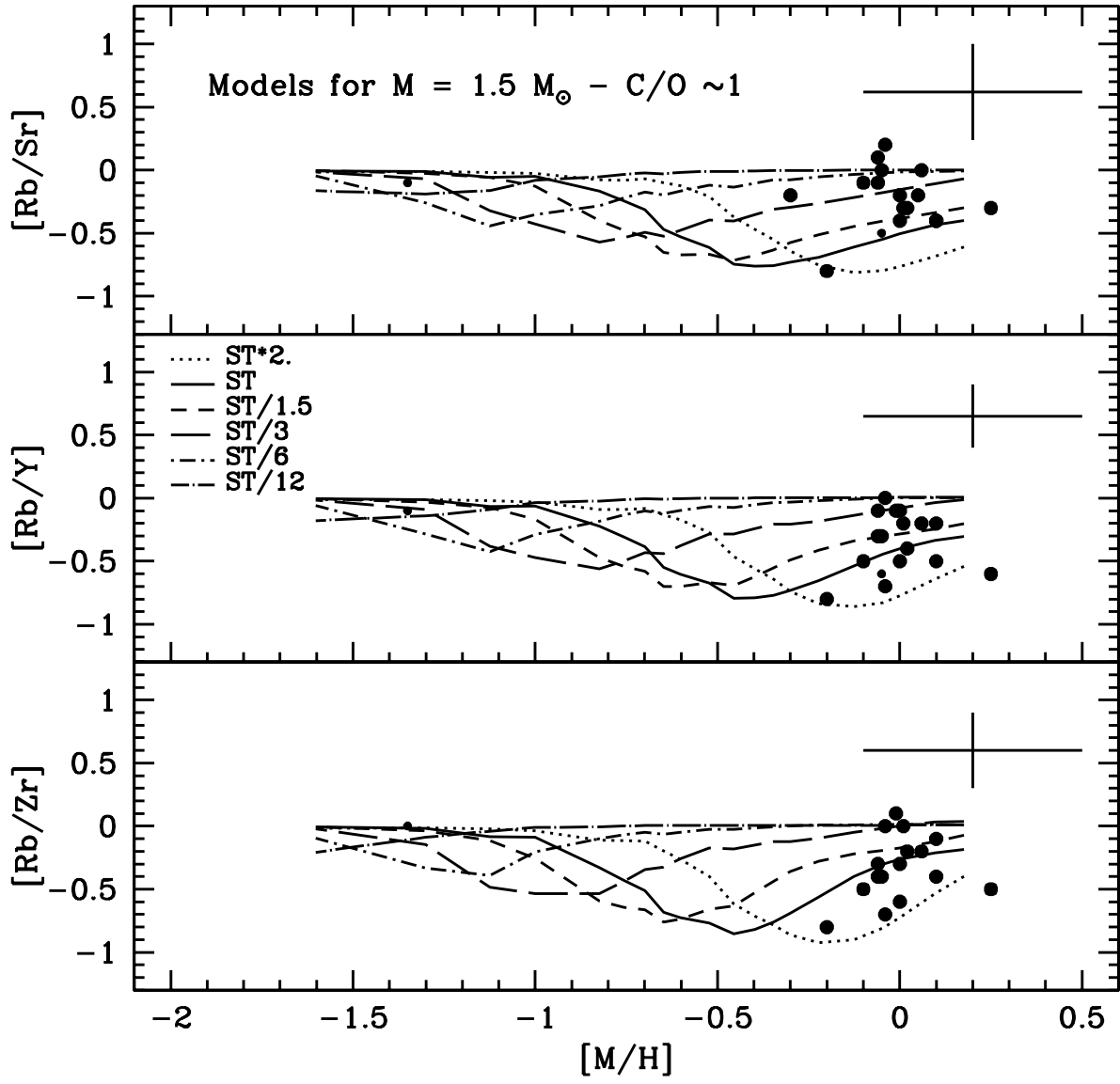
Fig. 4.— As Figure 3 comparing with theoretical predictions for a $5 M_{\odot}$ TP-AGB star.

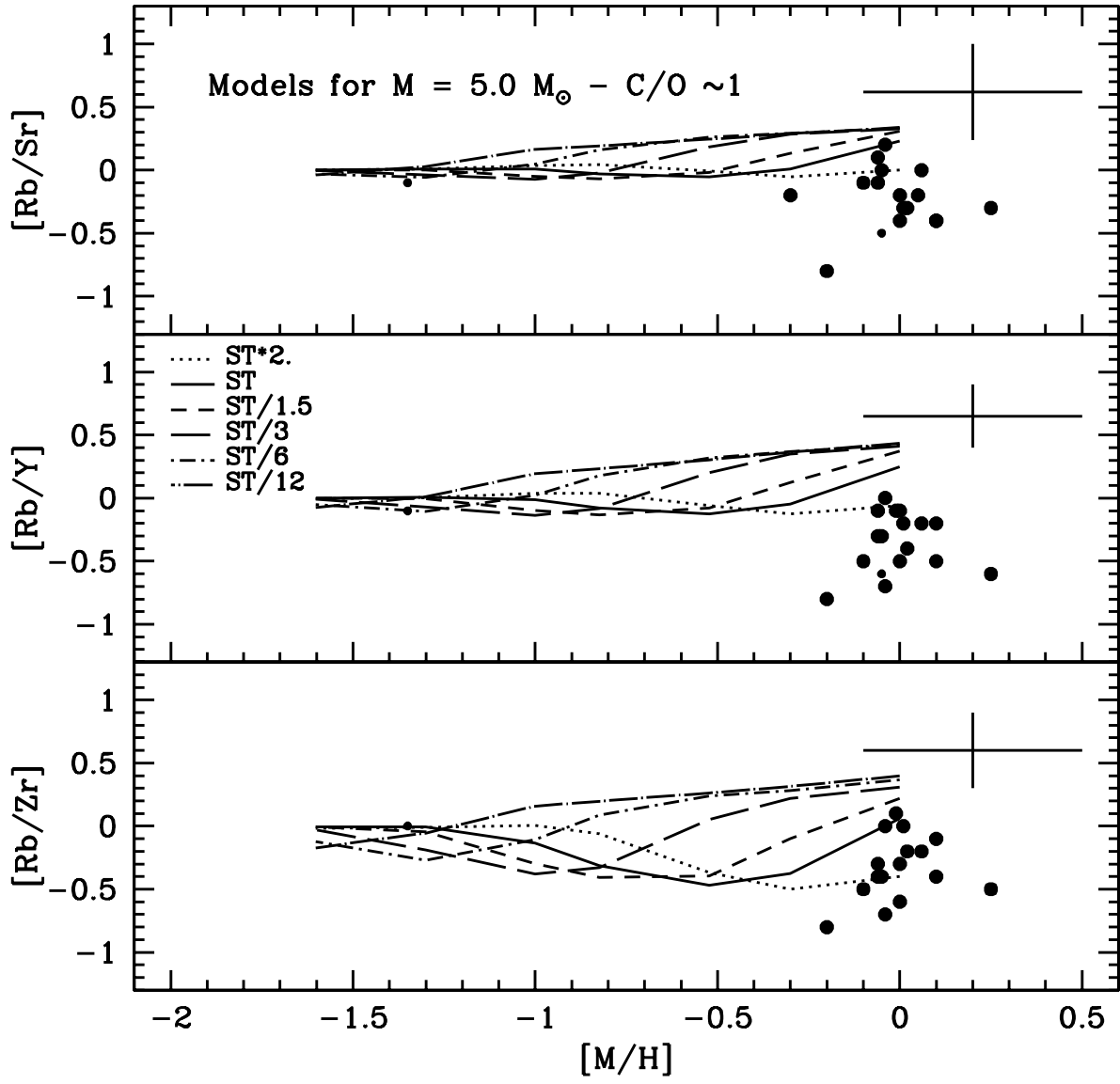
Fig. 5.— Comparison of the observed mean low-mass s-element (Y,Zr) enhancement (signature of the neutron exposure) against $[\text{Rb}/\text{Y}]$ (signature of the neutron density) with theoretical predictions for a $1.5 M_{\odot}$ (upper panel) and $5 M_{\odot}$ (lower panel) TP-AGB star for different parameterizations of the ^{13}C pocket (lines). The theoretical predictions shown are for stellar models with $C/O \sim 1$ and metallicity $[\text{Fe}/\text{H}] \gtrsim -0.3$, which is the metallicity of most of the stars studied here. Only stars in the sample with metallicity above this value are plotted (see text). Note that several stars coincide in the same data point.

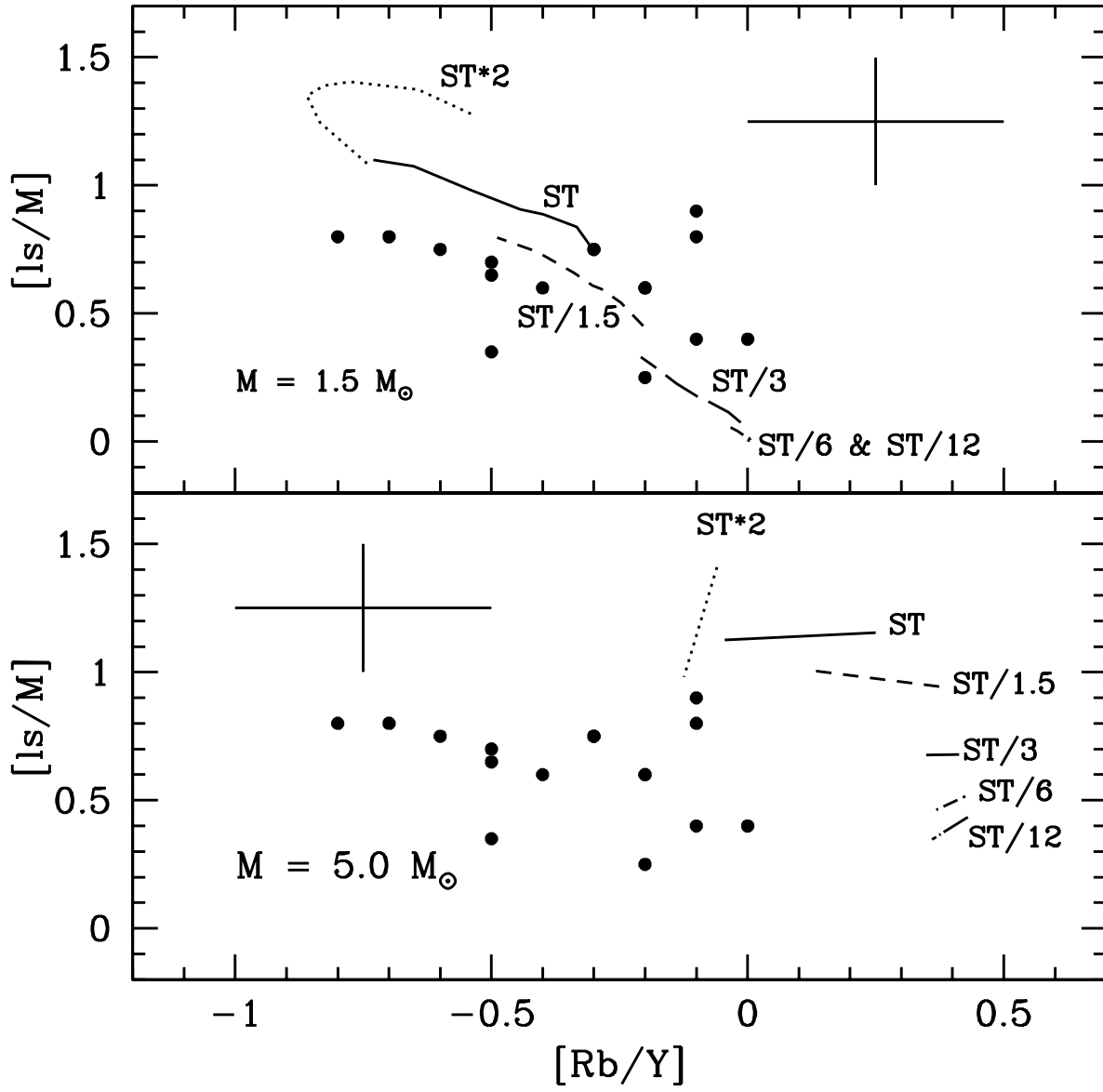
Fig. 6.— C/O vs. $^{12}\text{C}/^{13}\text{C}$ ratios derived in our stars. Note that most of the stars have a C/O ratio only slightly higher than 1 and that a significant number show $^{12}\text{C}/^{13}\text{C} < 40$. An average error bar is shown.











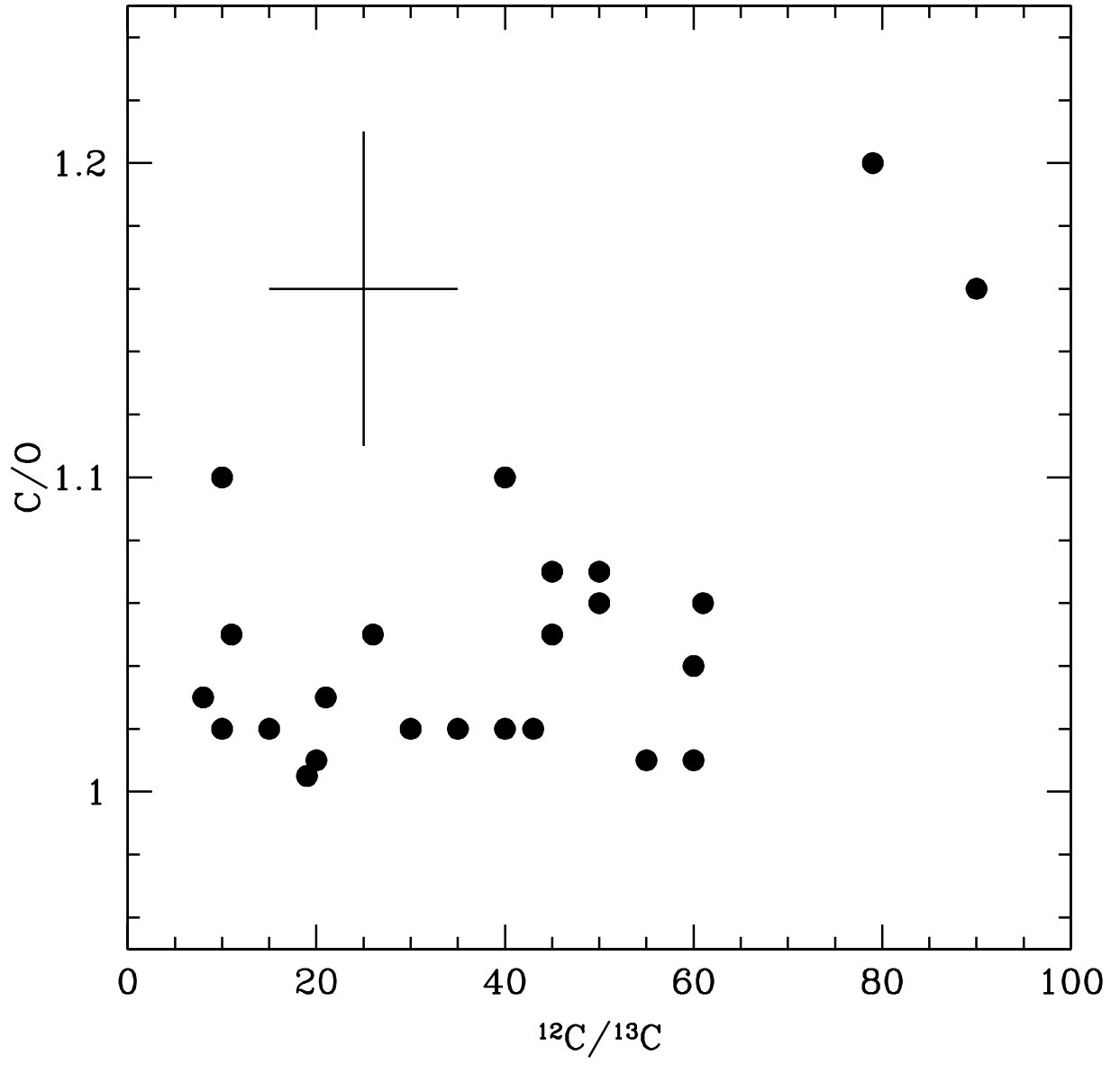


Table 3. Spectroscopic Data and Equivalent Widths

$\lambda(\text{\AA})$	$\chi(\text{eV})$	$\log gf$	AQ And	AW Cyg	EL Aur	HK Lyr	IRC –10397	IY Hya	LQ Cyg	RX Sct	S Sct	SY Per	SZ Sgr	TY Oph
CaI 6798.48	2.70	–2.320	200	...	<260	200	150	182	126	220	240	...
TiI 4503.75	2.13	–0.840
TiI 4759.63	2.17	–1.514	112	...
TiI 4801.94	0.83	–3.111	208	160	<190	160	170	160
TiI 4805.41	2.34	0.150	260	115	162	153	...	145	135
TiI 4812.89	0.84	–3.450	148	128	120
TiI 4821.27	2.16	–0.940
TiI 4870.12	2.24	0.518	186	...
TiI 4926.14	0.81	–2.170	...	197	270	<200
TiI 4937.72	0.81	–2.254
TiI 5238.53 ^b	2.09	–1.102	221	...	237	187	180
TiI 5238.58 ^b	0.85	–1.850
TiI 5716.48	2.29	–0.700	250	200	250	227	<300	<230	<240
TiI 7065.05	1.46	–2.609
V I 4748.50	2.04	–0.620
V I 5668.36	1.08	–1.030	...	<250	<300	234	185	...	260	<300	<260
V I 5670.85	1.08	–0.420	277	225

Table 3—Continued

$\lambda(\text{\AA})$	$\chi(\text{eV})$	$\log gf$	AQ And	AW Cyg	EL Aur	HK Lyr	IRC –10397	IY Hya	LQ Cyg	RX Sct	S Sct	SY Per	SZ Sgr	TY Oph	U Cam
FeI 4445.48	0.09	–5.441	278
FeI 4794.36	2.42	–4.050	...	118	92
FeI 4809.93	3.57	–2.720	100	90	...	40
FeI 4813.11	3.27	–2.890	77	80	88	...	97
FeI 4817.77	2.22	–3.530	80	...	140	125	110	110	119	...	113	100	158
FeI 4911.77	3.92	–1.687	51
FeI 5848.12	4.60	–0.903
NiI 4756.51	3.48	–0.340	120	100
CoI 4813.50	3.21	0.050	...	72	89	70	70	42	51	...	29	47	...
RbI 7800.23	0.00	0.130
SrI 4811.88	1.84	0.070	122	150
SrI 4872.45	1.79	–0.200
SrI 7070.10	1.84	–0.150
Y I 4780.18	1.88	–0.910	<260
Y I 4781.02	1.39	–0.460	120	150	126
Y I 4819.64	1.36	–0.480	140	100	120	140	150	145	120	...	155	134	140
Y I 4879.65	1.90	–0.400	100	...

Table 3—Continued

$\lambda(\text{\AA})$	$\chi(\text{eV})$	$\log gf$	AQ And	AW Cyg	EL Aur	HK Lyr	IRC –10397	IY Hya	LQ Cyg	RX Sct	S Sct	SY Per	SZ Sgr	TY Oph	U Car
Y I 8800.50	0.00	–2.240	362
ZrI 4772.32	0.62	0.040	280	<270
ZrI 4805.88	0.63	–0.420	190	220	210	200	200	185	198	215
ZrI 4815.03	0.65	–0.530
ZrI 4815.62	0.60	–0.630
ZrI 4828.05	0.62	–0.640	230	...	195	270	210 ...	180	200	...	250	202	185
ZrI 7849.39	0.68	–1.300	350
ZrI 8389.50	0.60	–1.760	360
TcI 5924.72	0.00	–2.440

^ahfs: hyperfine structure included; ss: spectrum synthesis used; s: solar gf derived; BG: Biémont et al. (1978); CB: Corliss (1962); FMW: Fuhr et al. (1988); HL: Hannaford et al. (1982); MFW: Martin, Fuhr, & Wiese (1988); NBS: Wiese & Fuhr (1962); Komarovskij (1991); No entry: Kurucz CD ROM No. 23 or VALD data bases.

^bThese two Ti I lines cannot be resolved. The equivalent width shown for the 5238.53 Å line corresponds to the width of the unresolved doublet. Obviously, we consider the contribution of the two lines in the abundance analysis.

Table 3. Continued

$\lambda(\text{\AA})$	UU Aur	UV Aql	UX Dra	V Aql	V CrB	V Oph	VX Gem	V460 Cyg	V781 Sgr	W Ori	Z Psc
CaI 6798.48	218	...	167	125	153	<250
TiI 4503.75	140
TiI 4759.63	96
TiI 4801.94	200	<190	151	220	...
TiI 4805.41	156	116	150	...	150	138
TiI 4812.89	146	115	108	115	110	...
TiI 4821.21	125
TiI 4870.12	180
TiI 4926.14	<230
TiI 4937.72	238	...
TiI 5238.53	<270	180	186	<265
TiI 5238.58
TiI 5716.48	...	264	157	...	170	<200	123	250	210	<270	...
TiI 7065.05
V I 4748.50	109	...
V I 5668.36	250	280	286	<270	<260	<285	<280
V I 5670.85	<240	208

Table 4. Dependence of Derived Abundances on Model Atmosphere Parameters

	$\log W_\lambda/\lambda$	$\Delta T_{\text{eff}} = \pm 200 \text{ K}$	$\Delta \xi = \pm 0.5 \text{ km s}^{-1}$	$\Delta C/O = \pm 0.05$	$\Delta^{12}\text{C}/^{13}\text{C} = \pm 10$	$\Delta \text{CNO}/\text{O}$
[Rb/H]	ss ^b	± 0.28	∓ 0.01	∓ 0.05	∓ 0.05	± 0.01
[Sr/H]	ss ^b	∓ 0.13	∓ 0.10	∓ 0.02	∓ 0.05	∓ 0.01
[Y/H]	-4.52	± 0.25	∓ 0.20	∓ 0.02	± 0.01	± 0.01
[Zr/H]	-4.39	± 0.15	∓ 0.30	∓ 0.05	± 0.01	± 0.01
[M/H]	-4.77	± 0.20	∓ 0.10	∓ 0.02	± 0.01	± 0.01

^aUncertainty due to a typical $\pm 20 \text{ m\AA}$ error in the equivalent widths. When spectral synthesis is used, this error in the placement of the spectral continuum.

^bThe abundances of Rb and Sr (in most of the stars) were derived using spectral synthesis (ss), see text.